

Advanced Radant Studies - II

B. L. J. Rao

This document is subject to special export controls and each transmittal to foreign governments or foreign nationals may be made only with prior approval of AFAL(AVWE-3) Wright-Patterson AFB, Ohio 45433.

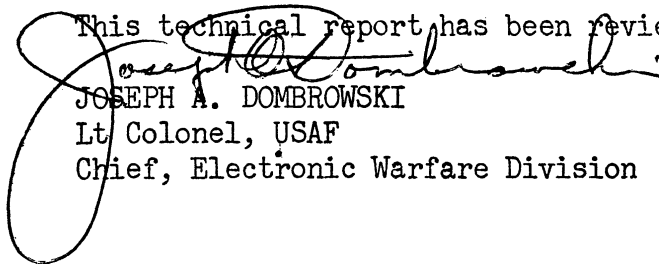
FOREWORD

This report was prepared by the University of Michigan Radiation Laboratory, Ann Arbor, Michigan 48108, under Contract No. F 33615-67-C-1444, Task 4161, Project 416102. The work was administered under the direction of the Air Force Avionics Laboratory (AVWE-3), Research and Technology Division, Air Force Systems Command: E.M. Turner, Technical Monitor, O.E. Horton, AVWE, Project Engineer.

This Final Technical Report covers the period from 1 February 1967 to 1 November 1967. The University of Michigan Report Number is 03664-1-F.

This report was submitted by the authors October 1967.

This technical report has been reviewed and is approved.



JOSEPH A. DOMBROWSKI
Lt Colonel, USAF
Chief, Electronic Warfare Division

ABSTRACT

The transmission characteristics of an anisotropic panel formed by conducting discs are investigated theoretically, for different orientation of the principal axis of the medium. The results indicate that the best transmission efficiency is obtained, for high incident angles, when the principal axis is oriented in such a way that it is perpendicular to the plane of the panel. It is shown by adjusting the orientation of the principal axis according to the incident angles, that better and more uniform transmission could be obtained through radomes of conical structure.

TABLE OF CONTENTS

I.	INTRODUCTION	1
II.	TENSOR PERMITTIVITY AND PERMEABILITY OF AN ARTIFICIAL ANISOTROPIC MEDIUM	3
III.	TRANSMISSION OF A PLANE ELECTROMAGNETIC WAVE THROUGH AN ANISOTROPIC PANEL	7
	3.1 Incident E-field Perpendicular to the Plane of Incidence (Perpendicular Polarization)	7
	3.2 Incident E-field Parallel to the Plane of Incidence (Parallel Polarization)	15
	3.3 Numerical Results	18
IV.	CONCLUSIONS AND RECOMMENDATIONS	56
	REFERENCES	57
	DD 1473	

LIST OF ILLUSTRATIONS

Fig. No.	Caption	Page
2-1	A Three-dimensional Array of Discs as an Artificial Anisotropic Medium.	3
3-1	Incident E-field Perpendicular to the Plane of Incidence	7
3-2	Incident E-field Parallel to the Plane of Incidence.	15
3-3	Reflection Coefficient $ r $ for $\epsilon_r=2, \epsilon_{1r}=3.3, \mu_{1r} = .755$	20
3-4	Brewster Angle θ_B vs α for $\mu_{1r} = .755, \epsilon_{1r} = 1.65, \epsilon_r=2; \epsilon_r=4$	21
3-5	Transmission Coefficient $ T ^2$ for $\epsilon_r=2, \epsilon_{1r}=3.3, \mu_{1r} = .755,$ ($d/\lambda = .04$).	22
3-6	Transmission Coefficient $ T ^2$ for $\epsilon_r=2, \epsilon_{1r}=3.3, \mu_{1r} = .755,$ ($d/\lambda = .05$).	23
3-7	Transmission Coefficient $ T ^2$ for $\epsilon_r=4, \epsilon_{1r}=6.6, \mu_{1r} = .755,$ ($d/\lambda = .04$).	24
3-8	Transmission Coefficient $ T ^2$ for $\epsilon_r=2, \epsilon_{1r}=3.3, \mu_{1r} = .755$ ($d/\lambda = .04$)	25
3-9	Transmission Coefficient $ T ^2$ for $\epsilon_r=2, \epsilon_{1r}=3.3, \mu_{1r} = .755$ ($d/\lambda = .05$)	26
3-10	Transmission Coefficient $ T ^2$ for $\epsilon_r=4, \epsilon_{1r}=6.6, \mu_{1r} = .755$ ($d/\lambda = .05$)	27
3-11	Transmission Coefficient $ T ^2$ for $\epsilon_r=2, \epsilon_{1r}=3.3, \mu_{1r} = .755$ $\alpha = 90^\circ$	28
3-12	Transmission Coefficient $ T ^2$ for $\epsilon_r=4, \epsilon_{1r}=6.6, \mu_{1r} = .755$ $\alpha = 90^\circ$.	29
3-13	Transmission Coefficient $ T ^2$ for $\epsilon_r=2, \epsilon_{1r}=3.3, \mu_{1r} = .755$ $\alpha=90^\circ$.	30
3-14	Transmission Coefficient $ T ^2$ for $\epsilon_r=4, \epsilon_{1r}=6.6, \mu_{1r} = .755,$ $\alpha = 90^\circ$	31
3-15	Conditions for Perfect Transmission ($ T ^2 = 1$) Through an Equivalent Half-wave Panel for $\epsilon_r=2, \epsilon_{1r}=3.3,$ $\mu_{1r} = .755$	33

(continued)

3-16	Conditions for Perfect Transmission ($ T ^2 = 1$) through an Equivalent Half-wave Panel for $\epsilon_r=4, \epsilon_{1r}=6.6, \mu_{1r}=.755$.	34
3-17	Conditions for Perfect Transmission ($ T ^2 = 1$) Through an Equivalent Half-wave Panel for $\epsilon_r=2, \epsilon_{1r}=3.3, \mu_{1r}=.755$	35
3-18	Conditions for Perfect Transmission ($ T ^2 = 1$) Through an Equivalent Half-wave Panel for $\epsilon_r=4, \epsilon_{1r}=6.6, \mu_{1r}=.755$	36
3-19	Transmission Coefficient $ T ^2$ for $\theta_t=60^\circ$ ($d_t/\lambda = .329$) $\epsilon_r=2, \epsilon_{1r}=3.3, \mu_{1r}=.755$	38
3-20	Transmission Coefficient $ T ^2$ for $\theta_t=70^\circ$ ($d_t/\lambda = .342$) $\epsilon_r=2, \epsilon_{1r}=3.3, \mu_{1r}=.755$	39
3-21	Transmission Coefficient $ T ^2$ for $\theta_t=80^\circ$ ($d_t/\lambda = .352$), $\epsilon_r=2, \epsilon_{1r}=3.3, \mu_{1r}=.755$.	40
3-22	Transmission Coefficient $ T ^2$ for $\theta_t = 60^\circ$ ($d_t/\lambda = .211$), $\epsilon_r=4, \epsilon_{1r}=6.6, \mu_{1r}=.755$	41
3-23	Transmission Coefficient $ T ^2$ for $\theta_t=70^\circ$ ($d_t/\lambda = .215$), $\epsilon_r=4, \epsilon_{1r}=6.6, \mu_{1r}=.755$	42
3-24	Transmission Coefficient $ T ^2$ for $\theta_t = 80^\circ$ ($d_t/\lambda = .217$), $\epsilon_r=4, \epsilon_{1r}=6.6, \mu_{1r}=.755$	43
3-25	Transmission Coefficient $ T ^2$ for $\theta_t = 60^\circ$ ($d_t/\lambda = .329$), $\epsilon_r=2, \epsilon_{1r}=3.3, \mu_{1r}=.755$	44
3-26	Transmission Coefficient $ T ^2$ for $\theta_t = 70^\circ$ ($d_t/\lambda = .342$), $\epsilon_r=2, \epsilon_{1r}=3.3, \mu_{1r}=.755$	45
3-27	Transmission Coefficient $ T ^2$ for $\theta_t = 80^\circ$ ($d_t/\lambda = .352$), $\epsilon_r=2, \epsilon_{1r}=3.3, \mu_{1r}=.755$	46
3-28	Transmission Coefficient $ T ^2$ for $\theta_t = 60^\circ$ ($d_t/\lambda = .211$), $\epsilon_r=4, \epsilon_{1r}=6.6, \mu_{1r}=.755$	47

(continued)

3-29	Transmission Coefficient $ T ^2$ for $\theta_t = 70^\circ$ ($d_t/\lambda = .215$), $\epsilon_r = 4$, $\epsilon_{1r} = 6.6$, $\mu_{1r} = .755$	48
3-30	Transmission Coefficient $ T ^2$ for $\theta_t = 80^\circ$ ($d_t/\lambda = .217$), $\epsilon_r = 4$, $\epsilon_{1r} = 6.6$, $\mu_{1r} = .755$	49
3-31	Transmission Coefficient $ T ^2$ for $\epsilon_r = 2$, $\epsilon_{1r} = 3.3$, $\mu_{1r} = .755$ $\alpha = 90^\circ$ and Various Values of θ_t	50
3-32	Transmission Coefficient $ T ^2$ for $\epsilon_r = 4$, $\epsilon_{1r} = 6.6$, $\mu_{1r} = .755$ $\alpha = 90^\circ$ and Various Values of θ_t	51
3-33	Transmission Coefficient $ T ^2$ for $\epsilon_r = 2$, $\epsilon_{1r} = 3.3$, $\mu_{1r} = .755$, $\alpha = 90^\circ$ and Various Values of θ_t	52
3-34	Transmission Coefficient $ T ^2$ for $\epsilon_r = 4$, $\epsilon_{1r} = 6.6$, $\mu_{1r} = .755$, $\alpha = 90^\circ$ and Various Values of θ_t	53
3-35	Anisotropic Conical Radome with Variable Principal Axis Orientation (α)	54
3-36	Transmission Coefficients $ T ^2$ and $ T ^2$ for $\epsilon_r = 4$, $\epsilon_{1r} = 6.6$, $\mu_{1r} = .755$, and $\theta_t = 80^\circ$ with α depending on θ	55

I

INTRODUCTION

The problem to be discussed here is an extension of the work previously reported.* Our aim is to find the effect of the orientation of the principal axis of an anisotropic panel on the transmission coefficients.

The problem discussed previously¹ is the transmission of a plane electromagnetic wave through an artificial anisotropic panel. The artificial dielectric which was under consideration consisted of arrays of small conducting discs whose planes are perpendicular to the interface of air and the panel. The resulting medium was double anisotropic (both permittivity and permeability are tensors) with the principal axis being parallel to one of the coordinate axes. The results of the analysis indicated that by properly adjusting the lattice parameters it is possible to change the transmission coefficient of the panel which cannot be accomplished by an isotropic panel. It was also noted that the double anisotropic panel offers the possibility of high transmission efficiency at incident angles near grazing. In the present study the above mentioned work is extended by considering the anisotropic medium consisting of arrays of discs which are arranged in such a way that the principal axis lies in a plane which is perpendicular to the plane of incidence. The problem studied previously becomes a special case of this more general problem.

Specifically, in Section II tensor permittivity and permeability are determined as a function of the orientation of the principal axis for the anisotropic medium under consideration. In the following section, the propagation constants in the anisotropic panel are first derived and then the power transmission coefficients are determined for the incident electric field is either perpendicular or parallel to the plane of incidence. In the final section, detailed numerical results are presented.

* See list of References for Radant Analysis Reports on the previous contract.

According to this study, it appears that the best transmission efficiency is obtained for high incident angles when the principal axis is oriented such that it is perpendicular to the plane of the panel. It is shown that by adjusting the orientation of the principal axis according to the incident angles, better and more uniform transmission could be obtained through radomes of conical structure.

II

TENSOR PERMITTIVITY AND PERMEABILITY OF AN ARTIFICIAL ANISOTROPIC MEDIUM

The artificial anisotropic medium is assumed to be made of arrays of disks embedded in a medium with permittivity and permeability denoted respectively by ϵ and μ_0 . The arrays of discs are arranged in such a way that the principal axis is pointed in x' direction, which makes an angle α with x -axis, as shown in Fig. 2-1.

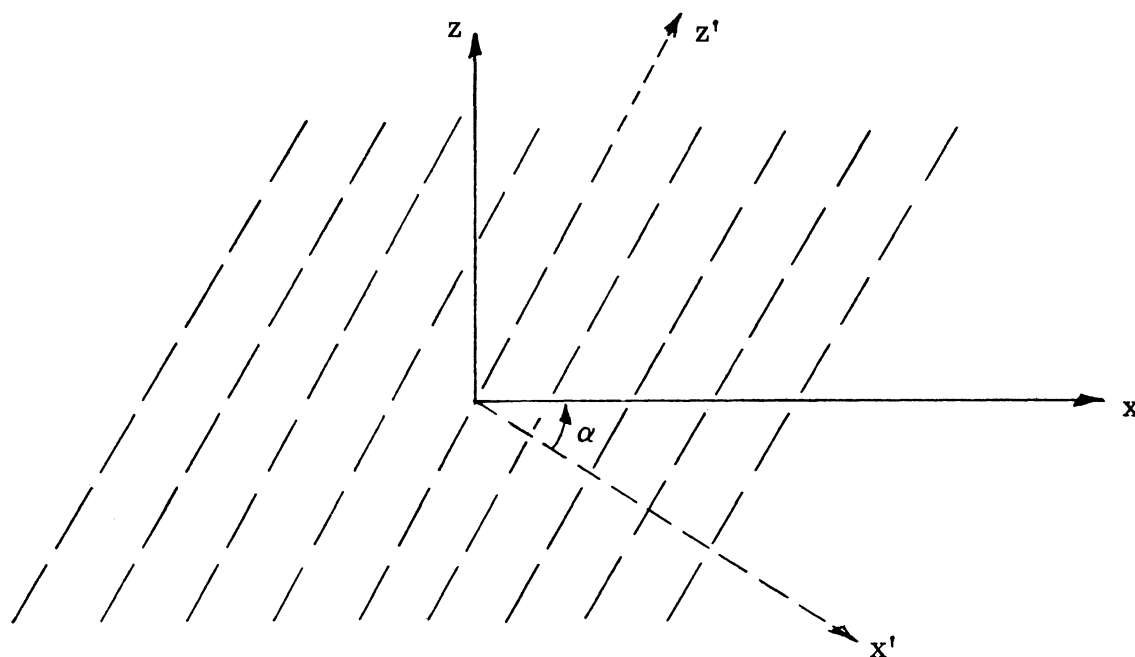


FIG. 2-1: A three dimensional array of disks as an artificial anisotropic medium.

In the previous work (C-T Tai, et al, 1965), the principal axis is assumed to be in x -direction (which becomes a special case ($\alpha = 0$) of the more general case considered here). In the primed coordinates, the constitutive relationships of the field vector are described by

$$\bar{\mathbf{D}}' = \bar{\boldsymbol{\epsilon}}' \cdot \bar{\mathbf{E}}' \quad (2.1)$$

$$\bar{\mathbf{B}}' = \bar{\boldsymbol{\mu}}' \cdot \bar{\mathbf{H}}' \quad (2.2)$$

where the permittivity and permeability tensors are defined by

$$\bar{\boldsymbol{\epsilon}}' = \begin{bmatrix} \epsilon & 0 & 0 \\ 0 & \epsilon_1 & 0 \\ 0 & 0 & \epsilon_1 \end{bmatrix} \quad (2.3)$$

$$\bar{\boldsymbol{\mu}}' = \begin{bmatrix} \mu_1 & 0 & 0 \\ 0 & \mu_0 & 0 \\ 0 & 0 & \mu_0 \end{bmatrix} \quad (2.4)$$

Formulae for ϵ_1 and μ_1 are found in the previous work (Tai, C-T, et al 1965).

Since the field vectors in the two systems transform according to the rule

$$\bar{\mathbf{A}}' = \bar{\mathbf{R}} \cdot \bar{\mathbf{A}} \quad (2.5)$$

where

$$\bar{\mathbf{R}} = \begin{bmatrix} \cos \alpha & 0 & -\sin \alpha \\ 0 & 1 & 0 \\ \sin \alpha & 0 & \cos \alpha \end{bmatrix} \quad (2.6)$$

one finds

$$\begin{aligned} \bar{\mathbf{D}} &= [\bar{\mathbf{R}}]^{-1} \cdot \bar{\mathbf{D}}' \\ &= [\bar{\mathbf{R}}]^{-1} \cdot \bar{\boldsymbol{\epsilon}}' \cdot \bar{\mathbf{E}}' \\ &= [\bar{\mathbf{R}}]^{-1} \cdot \bar{\boldsymbol{\epsilon}}' \cdot \bar{\mathbf{R}} \cdot \bar{\mathbf{E}} \end{aligned} \quad (2.7)$$

which shows that

$$D = \bar{\epsilon} \cdot \bar{E} \quad (2.8)$$

where $\bar{\epsilon} = [\bar{R}]^{-1} \cdot \bar{\epsilon}' \cdot \bar{R}$

$$= \begin{bmatrix} \epsilon \cos^2 \alpha + \epsilon_1 \sin^2 \alpha & 0 & (\epsilon_1 - \epsilon) \sin \alpha \cos \alpha \\ 0 & \epsilon_1 & 0 \\ (\epsilon_1 - \epsilon) \sin \alpha \cos \alpha & 0 & \epsilon \sin^2 \alpha + \epsilon_1 \cos^2 \alpha \end{bmatrix} \quad (2.9)$$

For later use it is convenient to represent

$$\epsilon_0 [\bar{\epsilon}]^{-1} = \begin{bmatrix} \xi_{11} & 0 & \xi_{13} \\ 0 & \xi_{22} & 0 \\ \xi_{31} & 0 & \xi_{33} \end{bmatrix}$$

$$= \begin{bmatrix} \frac{\epsilon_r \sin^2 \alpha + \epsilon_{1r} \cos^2 \alpha}{\epsilon_{1r} \epsilon_r} & 0 & \frac{(\epsilon_r - \epsilon_{1r}) \sin \alpha \cos \alpha}{\epsilon_{1r} \epsilon_r} \\ 0 & \frac{1}{\epsilon_{1r}} & 0 \\ \frac{(\epsilon_r - \epsilon_{1r}) \sin \alpha \cos \alpha}{\epsilon_{1r} \epsilon_r} & 0 & \frac{\epsilon_r \cos^2 \alpha + \epsilon_{1r} \sin^2 \alpha}{\epsilon_{1r} \epsilon_r} \end{bmatrix} \quad (2.10)$$

where $\epsilon_r = \frac{\epsilon}{\epsilon_0}$ and $\epsilon_{1r} = \frac{\epsilon_1}{\epsilon_0}$

Similarly,

$$\bar{\mathbf{B}} = \bar{\boldsymbol{\mu}} \cdot \bar{\mathbf{H}} \quad (2.11)$$

with

$$\begin{aligned} \bar{\boldsymbol{\mu}} &= [\bar{\mathbf{R}}]^{-1} \cdot \bar{\boldsymbol{\mu}}' \cdot \bar{\mathbf{R}} \\ &= \begin{bmatrix} \mu_1 \cos^2 \alpha + \mu_0 \sin^2 \alpha & 0 & (\mu_0 - \mu_1) \sin \alpha \cos \alpha \\ 0 & \mu_0 & 0 \\ (\mu_0 - \mu_1) \sin \alpha \cos \alpha & 0 & \mu_1 \sin^2 \alpha + \mu_0 \cos^2 \alpha \end{bmatrix} \end{aligned} \quad (2.12)$$

It is convenient, for later use, to represent

$$\begin{aligned} \mu_0 [\bar{\boldsymbol{\mu}}]^{-1} = \bar{\boldsymbol{\nu}} &= \begin{bmatrix} \nu_{11} & 0 & \nu_{13} \\ 0 & \nu_{22} & 0 \\ \nu_{31} & 0 & \nu_{33} \end{bmatrix} \\ &= \begin{bmatrix} \frac{\mu_1 \sin^2 \alpha + \mu_0 \cos^2 \alpha}{\mu_1} & 0 & \frac{(\mu_1 - \mu_0) \sin \alpha \cos \alpha}{\mu_1} \\ 0 & 1 & 0 \\ \frac{(\mu_1 - \mu_0) \sin \alpha \cos \alpha}{\mu_1} & 0 & \frac{\mu_1 \cos^2 \alpha + \mu_0 \sin^2 \alpha}{\mu_1} \end{bmatrix} \end{aligned} \quad (2.13)$$

III

TRANSMISSION OF PLANE ELECTROMAGNETIC WAVE THROUGH AN ANISOTROPIC PANEL

3.1 Incident E-field Perpendicular to the Plane of Incidence (Perpendicular Polarization)

We consider now the transmission of a plane electromagnetic wave through an anisotropic slab of thickness d as shown in Fig. 3-1.

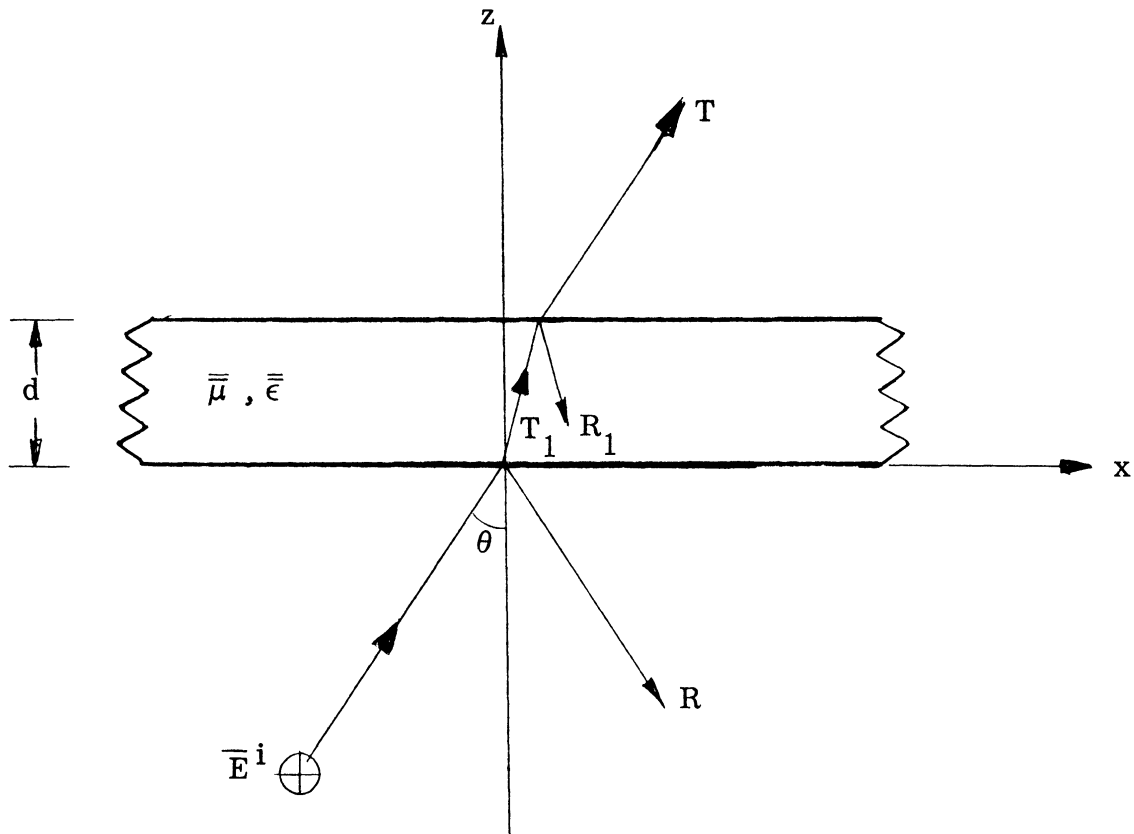


FIG. 3-1: Incident E-field Perpendicular to the Plane of Incidence

The Poynting vector of the plane incident wave makes an arbitrary angle θ with the normal to the interface. The tensor permittivity and permeability of the panel are the same as the ones defined by equations (2.9) and (2.12). The E-field of the incident wave is assumed to be in the y -direction.

Inside the slab, the fields satisfy the Maxwell's equation for harmonically varying field ($e^{j\omega t}$), which are given in terms of tensor permittivity and permeability, as

$$\nabla \cdot (\bar{\epsilon} \cdot \bar{E}) = 0 \quad (3.1)$$

$$\nabla \cdot (\bar{\mu} \cdot \bar{H}) = 0 \quad (3.2)$$

$$\nabla \times \bar{E} = -j \omega \bar{\mu} \cdot \bar{H} \quad (3.3)$$

$$\nabla \times \bar{H} = j \omega \bar{\epsilon} \cdot \bar{E} \quad (3.4)$$

The last two Maxwell's equations lead to the wave equations

$$\nabla \times \left([\bar{\mu}]^{-1} \cdot \nabla \times \bar{E} \right) - \omega^2 \bar{\epsilon} \cdot \bar{E} = 0 \quad (3.5)$$

$$\nabla \times \left([\bar{\epsilon}]^{-1} \cdot \nabla \times \bar{H} \right) - \omega^2 \bar{\mu} \cdot \bar{H} = 0 \quad (3.6)$$

The sharp boundaries of the slab (see Fig. 3-1) imposes the following two constraints on the solution of the wave equation. Within the slab, the fields must be related to the fields on the interface so they must not vary as a function of y (i.e. $\partial/\partial y=0$). In addition, the phase velocity of the wave in the x -direction must be the same as the phase velocity in the x -direction at the interface. Because of these two constraints, the y and x dependence of the wave equation is specified. It is only necessary to solve for the remaining z dependence. The fields in the anisotropic slab can thus be written in the form (for E -vector polarized in the y -direction)

$$\bar{E} = E_1 e^{-j(\bar{K} \cdot \bar{r})} \quad (3.7)$$

where

$$\bar{K} = \hat{x} K_x + \hat{z} K_z$$

$$\bar{r} = \bar{x} + \bar{z}$$

and

$$K_x = K_o \sin \theta$$

with K_o being the usual free space wave number.

By substituting equation (3.7) in equation (3.5) one finds

$$\left(K_z^2 \nu_{22} - K_o^2 \frac{\epsilon_{11}}{\epsilon_o} \right) E_x + \left(-K_x K_z \nu_{22} - K_o^2 \frac{\epsilon_{13}}{\epsilon_o} \right) E_z = 0 \quad (3.8)$$

$$\left(K_x^2 \nu_{33} + K_z^2 \nu_{11} - K_x K_z (\nu_{31} + \nu_{13}) - K_o^2 \frac{\epsilon_{22}}{\epsilon_o} \right) E_y = 0 \quad (3.9)$$

$$\left(-K_x K_z \nu_{22} - K_o^2 \frac{\epsilon_{31}}{\epsilon_o} \right) E_x + \left(K_x^2 \nu_{22} - K_o^2 \frac{\epsilon_{33}}{\epsilon_o} \right) E_z = 0 \quad (3.10)$$

where the ϵ 's are the coefficients of the dielectric constant tensor ϵ as given in equation (2.9).

The non-trivial solution of the above three equations is evidently given by

$$K_x^2 \nu_{33} + K_z^2 \nu_{11} - K_x K_z (\nu_{31} + \nu_{13}) - K_o^2 \frac{\epsilon_{22}}{\epsilon_o} = 0 \quad (3.11)$$

Noting that $\nu_{31} = \nu_{13}$ and $\frac{\epsilon_{22}}{\epsilon_o} = \epsilon_{1r}$, we obtain from equation (3.11) the following characteristic equation which must be satisfied by K_x and K_z .

$$\nu_{11} K_z^2 - 2\nu_{13} K_x K_z + \nu_{33} K_x^2 - K_o^2 \epsilon_{1r} = 0 \quad (3.12)$$

where ν_{11} , ν_{13} and ν_{33} are the elements of the tensor $\mu_o [\bar{\mu}]^{-1}$ and are given by equation (2.13).

Equation (3.12) represents a quadratic equation in K_z , the corresponding two solutions are given by

$$K_z = \frac{\nu_{13} K_x \pm \sqrt{K_x^2 (\nu_{13}^2 - \nu_{11} \nu_{33}) + K_o^2 \nu_{11} \epsilon_{1r}}}{\nu_{11}} \quad (3.13)$$

The value of K_z with positive sign before the square root represents the propagation constant in the positive z -direction and is represented by

$$K_{z+} = \frac{\nu_{13} K_x + P}{\nu_{11}} \quad (3.14)$$

where

$$P = \sqrt{K_x^2 (\nu_{13}^2 - \nu_{11} \nu_{33}) + K_o^2 \nu_{11} \epsilon_{1r}}$$

The value of K_z with negative sign before the square root represents the negative of propagation constant in the negative z -direction. Thus, if k_{z-} represents the propagation constant in the negative z -direction, it is given by

$$K_{z-} = \frac{-\nu_{13} K_x + P}{\nu_{11}} \quad (3.15)$$

Having determined the propagation constants in the anisotropic slab, the general expressions for the fields in the three regions are given by:

Region 1, $z \leq 0$

$$\bar{E}^i = E_o \hat{y} e^{-j(K_x x + K_{zo} z)} \quad (3.16)$$

$$\bar{H}^i = \frac{E_o}{\omega \mu_o} \left(-\hat{x} K_{zo} + \hat{z} K_x \right) e^{-j(K_x x + K_{zo} z)} \quad (3.17)$$

where

$$K_x = K_o \sin \theta, \quad K_{zo} = K_o \cos \theta \quad \text{and} \quad K_o = \frac{2\pi}{\lambda}$$

$$\bar{E}^r = RE_o \hat{y} e^{-j(K_x x - K_{zo} z)} \quad (3.18)$$

$$\bar{H}^r = \frac{RE_o}{\omega \mu_o} \left(\hat{x} K_{zo} + \hat{z} K_x \right) e^{-j(K_x x - K_{zo} z)} \quad (3.19)$$

Region 2, $0 \leq z \leq d$

$$\bar{E}^d = E_o \hat{y} \left[T_1 e^{-j(K_x x + K_{z+} z)} + R_1 e^{-j(K_x x - K_{z-} z)} \right] \quad (3.20)$$

$$\begin{aligned} \bar{H}^d = \frac{E_o}{\omega} \left[\bar{\mu} \right]^{-1} & \left[T_1 \left(-K_{z+} \hat{x} + K_x \hat{z} \right) e^{-j(K_x x + K_{z+} z)} \right. \\ & \left. + R_1 \left(K_{z-} \hat{x} + K_x \hat{z} \right) e^{-j(K_x x - K_{z-} z)} \right] \end{aligned} \quad (3.21)$$

where K_{z+} and K_{z-} are given by equations (3.14) and (3.15). $\left[\bar{\mu} \right]^{-1}$ is the inverse of μ and is given by equation (2.13).

Region 3, $z \geq d$

$$\bar{E}^t = T E_0 \hat{y} e^{-j(K_x x + K_{z0} z)} \quad (3.22)$$

$$\bar{H}^t = \frac{T E_0}{\omega \mu_0} \left(-K_{z0} \hat{x} + K_x \hat{z} \right) e^{-j(K_x x + K_{z0} z)} \quad (3.23)$$

By matching the tangential components of the E and H fields at the two interfaces, corresponding to $z = 0$ and $z = d$, one can determine unknown coefficients T_1 , R_1 , T and R using the equations (3.16) to (3.23). The results are given below.

$$T_1 = \frac{2 K_{z0} / (K_{z0} + \nu_{11} K_{z+} - \nu_{13} K_x)}{1 - r_1 r_2 e^{-j(K_{z+} + K_{z-})d}} \quad (3.24)$$

$$R_1 = -T_1 r_1 e^{-j(K_{z+} + K_{z-})d} \quad (3.25)$$

$$R = -1 + T_1 \left[1 - r_1 e^{-j(K_{z+} + K_{z-})d} \right] \quad (3.26)$$

and

$$T = T_1 (1 - r_1) e^{-j(K_{z+} - K_{z0})d} \quad (3.27)$$

where

$$r_1 = \frac{-\nu_{11} K_{z+} + \nu_{13} K_x + K_{z0}}{\nu_{11} K_{z-} + \nu_{13} K_x + K_{z0}} \quad (3.28)$$

$$r_2 = \frac{-\nu_{11} K_{z-} - \nu_{13} K_x + K_{z0}}{\nu_{11} K_{z+} - \nu_{13} K_x + K_{z0}} \quad (3.29)$$

From equations (3.14) and (3.15) it is noted that

$$\nu_{11} K_{z+} - \nu_{13} K_x = P \quad (3.30)$$

$$\nu_{11} K_{z-} + \nu_{13} K_x = P \quad (3.31)$$

Adding the above two equations results in

$$K_{z+} + K_{z-} = \frac{2P}{\nu_{11}} \quad (3.32)$$

Using the relations in equations (3.30) to (3.32), the expressions for the coefficients T_1 , R_1 , R and T could be expressed in a compact form, the results are summarized below

$$T_1 = \frac{1+r}{1-r^2 e^{-j2 \frac{P}{\nu_{11}} d}} \quad (3.33)$$

$$R_1 = \frac{r(1+r) e^{-j2 \frac{P}{\nu_{11}} d}}{1-r^2 e^{-j2 \frac{P}{\nu_{11}} d}} \quad (3.34)$$

$$R = \frac{r(1 - e^{-j2 \frac{P}{\nu_{11}} d})}{1-r^2 e^{-j2 \frac{P}{\nu_{11}} d}} \quad (3.35)$$

and

$$T = \frac{(1 - r^2) e^{-j(K_z + -K_{z0})d}}{1 - r^2 e^{-j \frac{2P}{\nu_{11}} d}} \quad (3.36)$$

where $r = r_1 = r_2 = \frac{K_{z0} - P}{K_{z0} + P}$ (3.37)

$$P = \sqrt{K_o^2 \nu_{11} \epsilon_{1r} - \frac{K_x^2}{\mu_{1r}}} \quad (3.38)$$

and $\mu_{1r} = \frac{\mu_1}{\mu_o}$

Since the interest is mainly in the magnitude of power transmission coefficient $|T|^2$, it can easily be verified that

$$|T|^2 = \frac{1}{1 + \left[\frac{2r \sin\left(\frac{P}{\nu_{11}} d\right)}{1 - r^2} \right]^2} \quad (3.39)$$

From equation (3.39), it is evident that perfect transmission ($|T|^2 = 1$) is obtained when $\frac{P}{\nu_{11}} d$ is equal to an integral multiple of π . We consider later the case when $\frac{P}{\nu_{11}} d = \pi$. It is also noted from equation (3.39) that the transmission efficiency increases as the value of r decreases. For given ϵ_1 and μ_1 , it can easily be verified that r will have the least value when $\alpha = 90^\circ$, for any given value of θ . These comments will be explored in more detail in the final section.

3.2 Incident E-field Parallel to the Plane of Incidence (Parallel Polarization)

We consider now the transmission of a plane electromagnetic wave through an anisotropic slab of thickness d , when the incident E-field is parallel to the plane of incidence, as shown in Fig. 3-2.

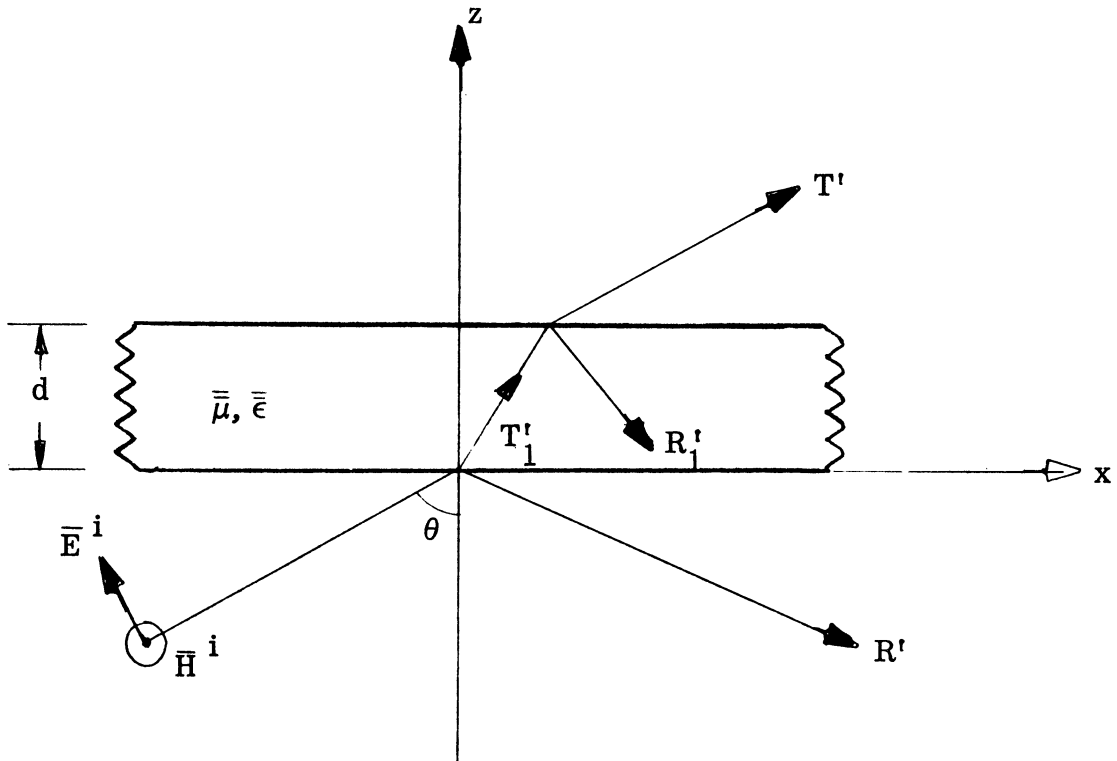


FIG. 3-2: Incident E-field parallel to the plane of incidence.

The tensor permittivity and permeability of the panel are the same as the ones defined by equations (2.9) and (2.12).

In the present case the plane wave is characterized by a H_y component such that

$$H_y = H_0 \hat{y} e^{-j(\bar{K}^i \cdot \bar{r})} \quad (3.40)$$

where

$$\bar{K}' = K_x \hat{x} + K'_z \hat{z}$$

By substituting (3.40) into the corresponding wave equation given by equation (3.6) which is repeated below for convenience,

$$\nabla_x \left(\left[\bar{\epsilon} \right]^{-1} \cdot \nabla_x \bar{H} \right) - \omega^2 \bar{\mu} \bar{H} = 0$$

one finds that K_x and K'_z must satisfy the following characteristic equation,

$$\xi_{11} K_z'^2 - 2 \xi_{13} K_x K'_z + \xi_{33} K_x^2 - K_0^2 = 0 \quad (3.41)$$

By solving equation (3.41) it is not difficult to show that the propagation constants in the positive and negative z -direction are respectively given by

$$K_{z+}' = \frac{\xi_{13} K_x + P'}{\xi_{11}} \quad (3.42)$$

$$K_{z-}' = \frac{-\xi_{13} K_x + P'}{\xi_{11}} \quad (3.43)$$

where

$$P' = \sqrt{K_0^2 \xi_{11} - \frac{K_x^2}{\epsilon_r \epsilon_{1r}}}$$

and ξ 's are the coefficients of the $\epsilon_0 \left[\bar{\epsilon} \right]^{-1}$ and are given by equation (2.10). Having determined the propagation constant, it is convenient to define the reflection and the transmission coefficients with reference to the incident magnetic field, and the general expressions for the electromagnetic field in the different regions are given by,

Region 1, $z \leq 0$

$$\bar{H}^i = H_o \hat{y} e^{-j(K_x x + K_{zo} z)} \quad (3.44)$$

$$\bar{E}^i = \frac{H_o}{\omega \epsilon_o} \left(K_{zo} \hat{x} - K_x \hat{z} \right) e^{-j(K_x x + K_{zo} z)} \quad (3.45)$$

where $K_x = K_o \sin \theta$, $K_{zo} = K_o \cos \theta$, and $K_o = \frac{2\pi}{\lambda}$.

$$\bar{H}^r = R' H_o \hat{y} e^{-j(K_x x - K_{zo} z)} \quad (3.46)$$

$$\bar{E}^r = \frac{R' H_o}{\omega \epsilon_o} \left(-K_{zo} \hat{x} - K_x \hat{z} \right) e^{-j(K_x x - K_{zo} z)} \quad (3.47)$$

Region 2, $0 \leq z \leq d$

$$\bar{H}^d = H_o \hat{y} \left[T'_1 e^{-j(K_x x + K'_{z+} z)} + R'_1 e^{-j(K'_x x - K'_{z-} z)} \right] \quad (3.48)$$

$$\begin{aligned} \bar{E}^d = \frac{H_o}{\omega} [\bar{\epsilon}]^{-1} & \left[T'_1 \left(K'_{z+} \hat{x} - K_x \hat{z} \right) e^{-j(K_x x + K'_{z+} z)} \right. \\ & \left. + R'_1 \left(-K'_{z-} \hat{x} - K_x \hat{z} \right) e^{-j(K_x x - K'_{z-} z)} \right] \end{aligned} \quad (3.49)$$

Region 3, $z \geq d$

$$\bar{H}^t = T' H_o \hat{y} e^{-j(K_x x + K_{zo} z)} \quad (3.50)$$

$$\bar{E}^t = \frac{T^1 H_0}{\omega \epsilon_0} \left(K_{z0} \hat{x} - K_x \hat{z} \right) e^{-j \left(K_x x + K_{z0} z \right)} \quad (3.51)$$

By matching the tangential components of the E and H fields at the two interfaces, corresponding to $z = 0$ and $z = d$, one can determine the unknown coefficients T_1^t , R_1^t , T^t and R^t as we did in the case of the perpendicular polarization. The results have the same algebraic forms as those given by equations (3.33) to (3.36) except that the coefficients K_{z+} , K_{z-} , P , r and ν 's are replaced, respectively by K'_{z+} , K'_{z-} , P' , r' and ξ 's. The expressions for K'_{z+} , K'_{z-} , P' and ξ 's are given in equations (3.42), (3.43) and (2.10). The expression for r' is as defined below

$$r' = \frac{K_{z0} - P'}{K_{z0} + P'} \quad (3.52)$$

Thus, the expression for $|T^t|^2$, which is our main interest, is given by

$$|T^t|^2 = \frac{1}{1 + \left[\frac{2 r' \sin \left(\frac{P' d}{\xi_{11}} \right)}{1 - r'^2} \right]^2} \quad (3.53)$$

3.3 Numerical Results

As stated in the introduction, our aim is to study the effect of α (which represents the orientation of the principal axis of the anisotropic panel) on the transmission of a plane wave through an anisotropic panel. To this end, we note, from the expression of power transmissions coefficients given by equation (3.39) and (3.53), that the transmission efficiency increases as the values of r and r' decreases. From the expressions of r , it could be noted that the value of r decreases with the increase

in α for any given angle of incidence θ , and has the minimum value when $\alpha = \frac{\pi}{2}$. This can easily be noted from the computed values of r as shown in Fig. 3-3. From the expressions of r' , it can be noted that it becomes zero for a certain incident angle θ_B , which is usually called the Brewster angle and is given by

$$\cos \theta_B = \sqrt{\frac{(\epsilon_r - 1) \sin^2 \alpha + (\epsilon_{1r} - 1) \cos^2 \alpha}{\epsilon_r \epsilon_{1r} - 1}} \quad (3.54)$$

For this incident angle $|T'|^2 = 1$, indicating a perfect transmission. It can easily be noted either from equation (3.54) or from Fig. 3-4, that θ_B increases with α and has maximum value for $\alpha = \frac{\pi}{2}$, provided ϵ_r and ϵ_{1r} remains the same. This indicates that better transmission is obtained for high angles of incidence when $\alpha = \frac{\pi}{2}$.

Figures 3-5 to 3-7 represent the computed transmission coefficient $|T|^2$ for different values of α , for several thicknesses of the panel $\left(\frac{d}{\lambda} \ll 1\right)$ and for two sets of values for ϵ_r and ϵ_{1r} . Similarly the Figs. 3-8 to 3-10 represent $|T'|^2$ as a function α . From these computed results for thin panel, it is evident that better transmission is obtained when $\alpha = \frac{\pi}{2}$, especially for high angles of incidence which is of interest for radomes characterized by high fineness ratio. Having noted that $\alpha = \frac{\pi}{2}$ gives better transmission, the transmission coefficients are computed for several thicknesses of the panel $\left(\frac{d}{\lambda} \ll 1\right)$ and are plotted in Figs. 3-11 to 3-14. These results will be of interest to see how the transmission changes with frequency.

Now, it is of some interest to point out the special characteristics of transparent panels at oblique incidence. From equations (3.49) and (3.53) we see that $|T|^2$ becomes unity when

$$\frac{Pd}{\nu_{11}} = N \pi \quad (3.55)$$

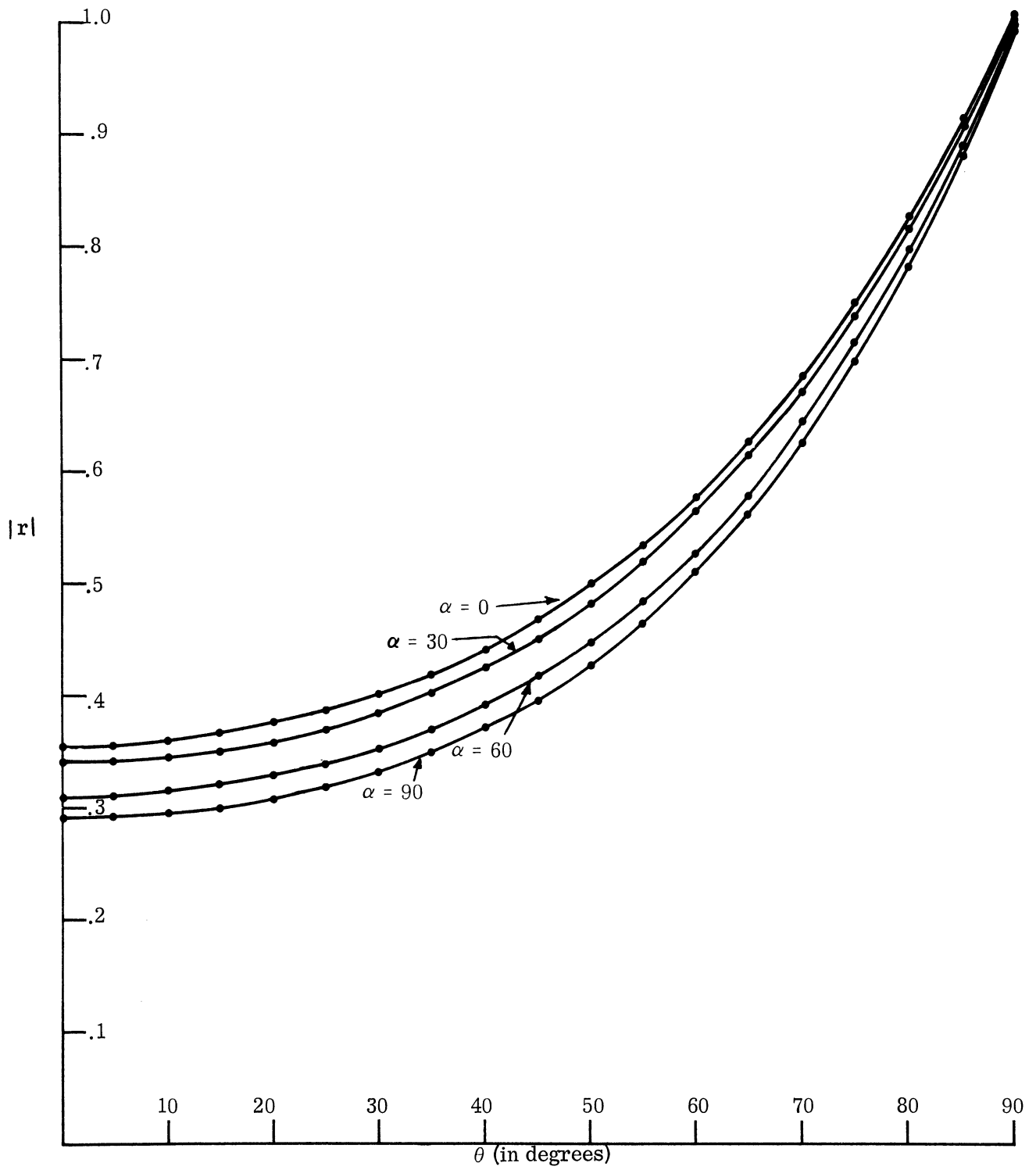


FIG. 3-3: REFLECTION COEFFICIENT $|r|$ for $\epsilon_r=2$, $\epsilon_{1r}=3.3$, $\mu_{1r}=.755$.

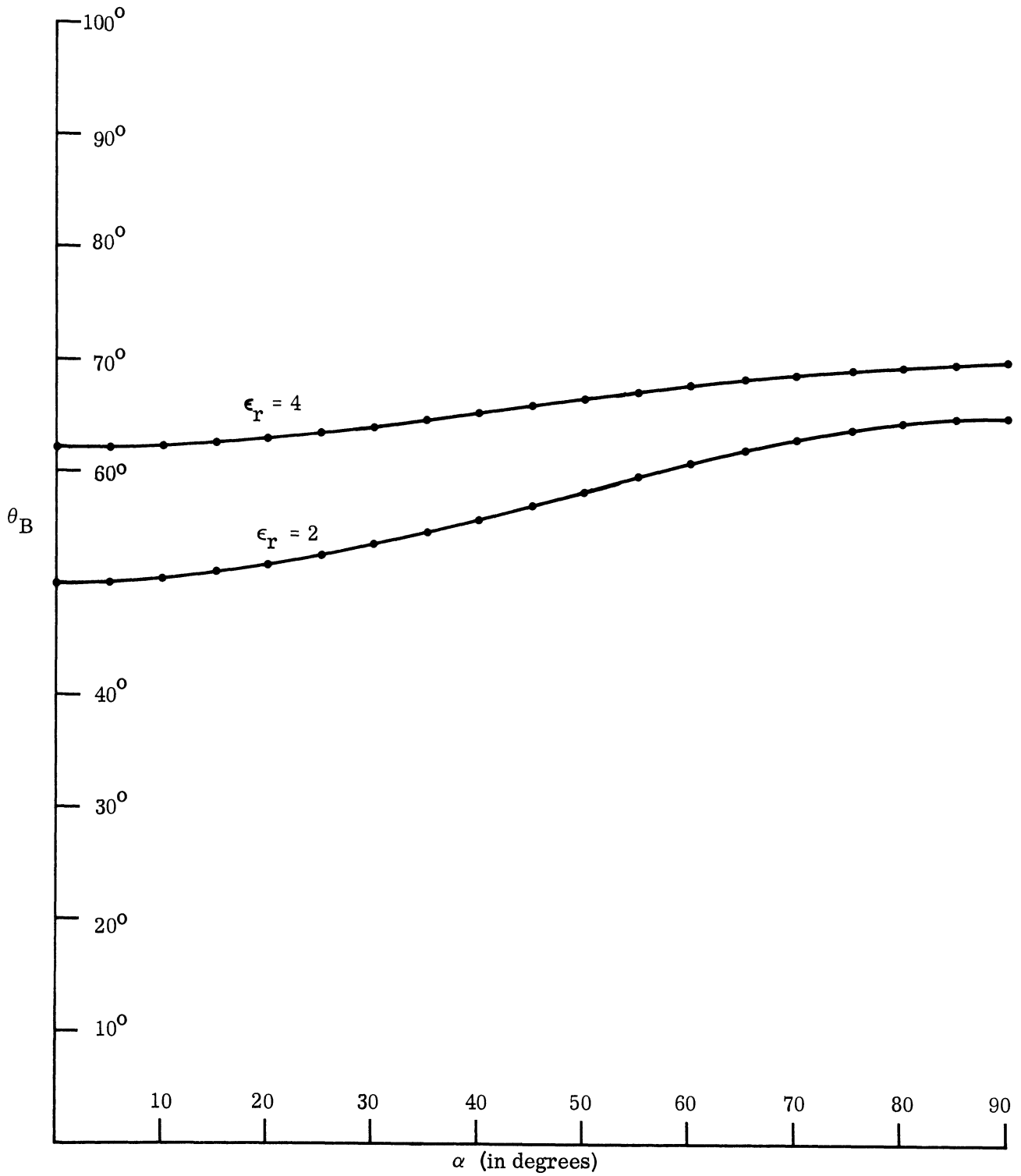


FIG. 3-4: BREWSTER ANGLE θ_B VS α FOR $\mu_{1r} = .755$, $\epsilon_{1r} = 1.65$, $\epsilon_r = 2$, $\epsilon_r = 4$.

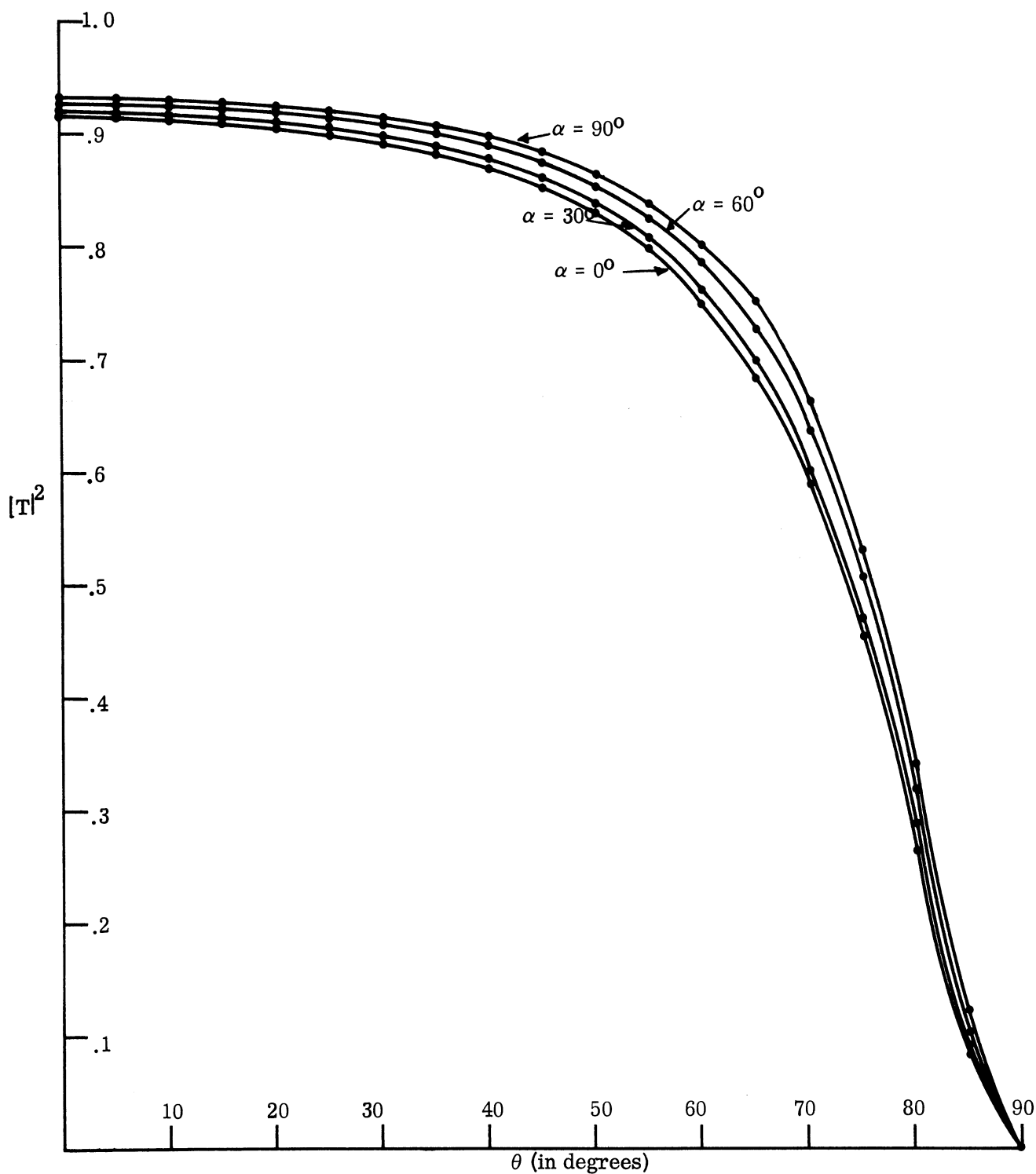


FIG. 3-5: TRANSMISSION COEFFICIENT $|T|^2$ FOR $\epsilon_r=2, \epsilon_{1r}=3.3, \mu_{1r}=.755,$
 $(d/\lambda=.04)$.

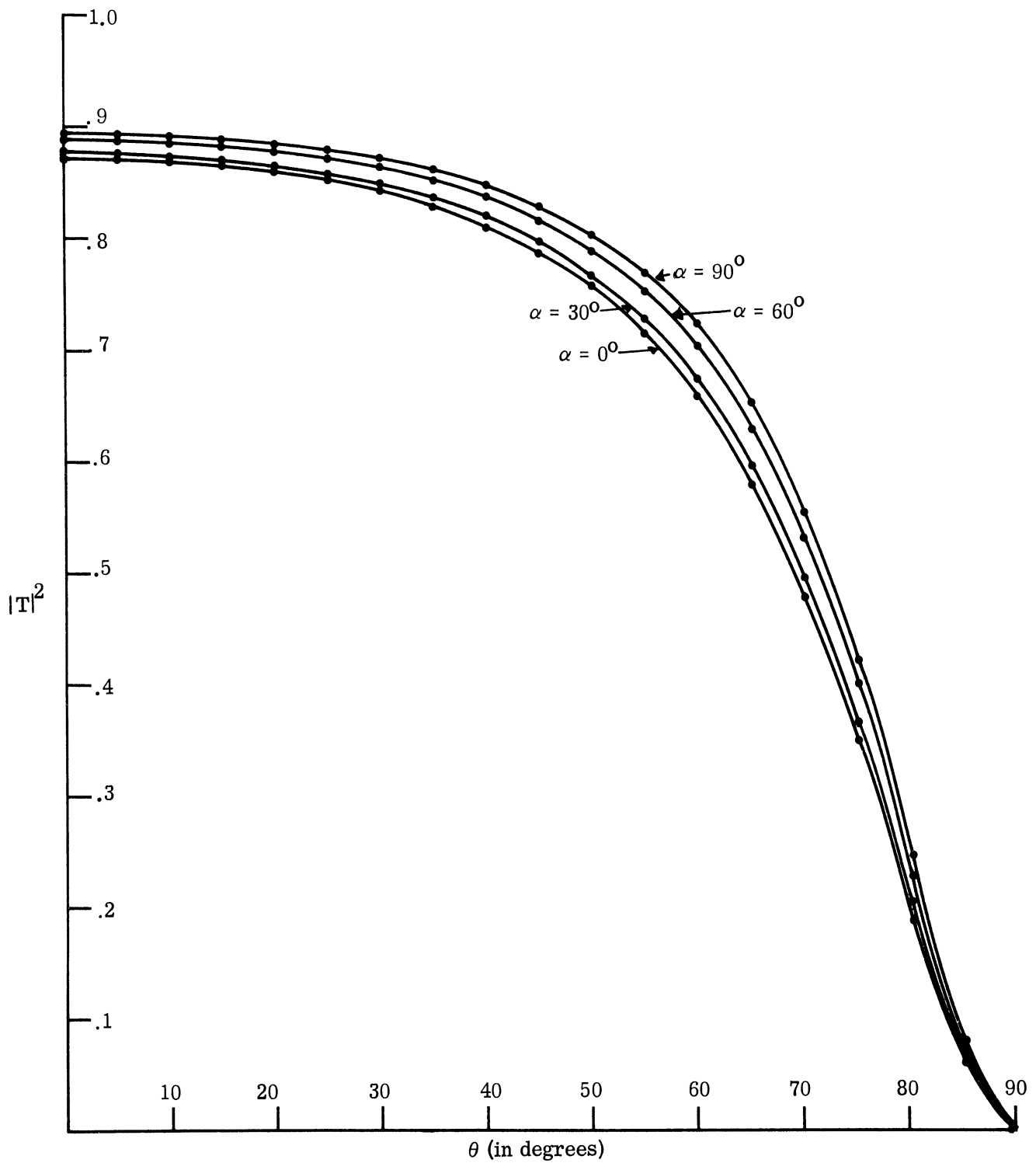


FIG. 3-6: TRANSMISSION COEFFICIENT $|T|^2$ FOR $\epsilon_r = 2$, $\epsilon_{1r} = 3.3$, $\mu_{1r} = .755$,
 ($d/\lambda = .05$).

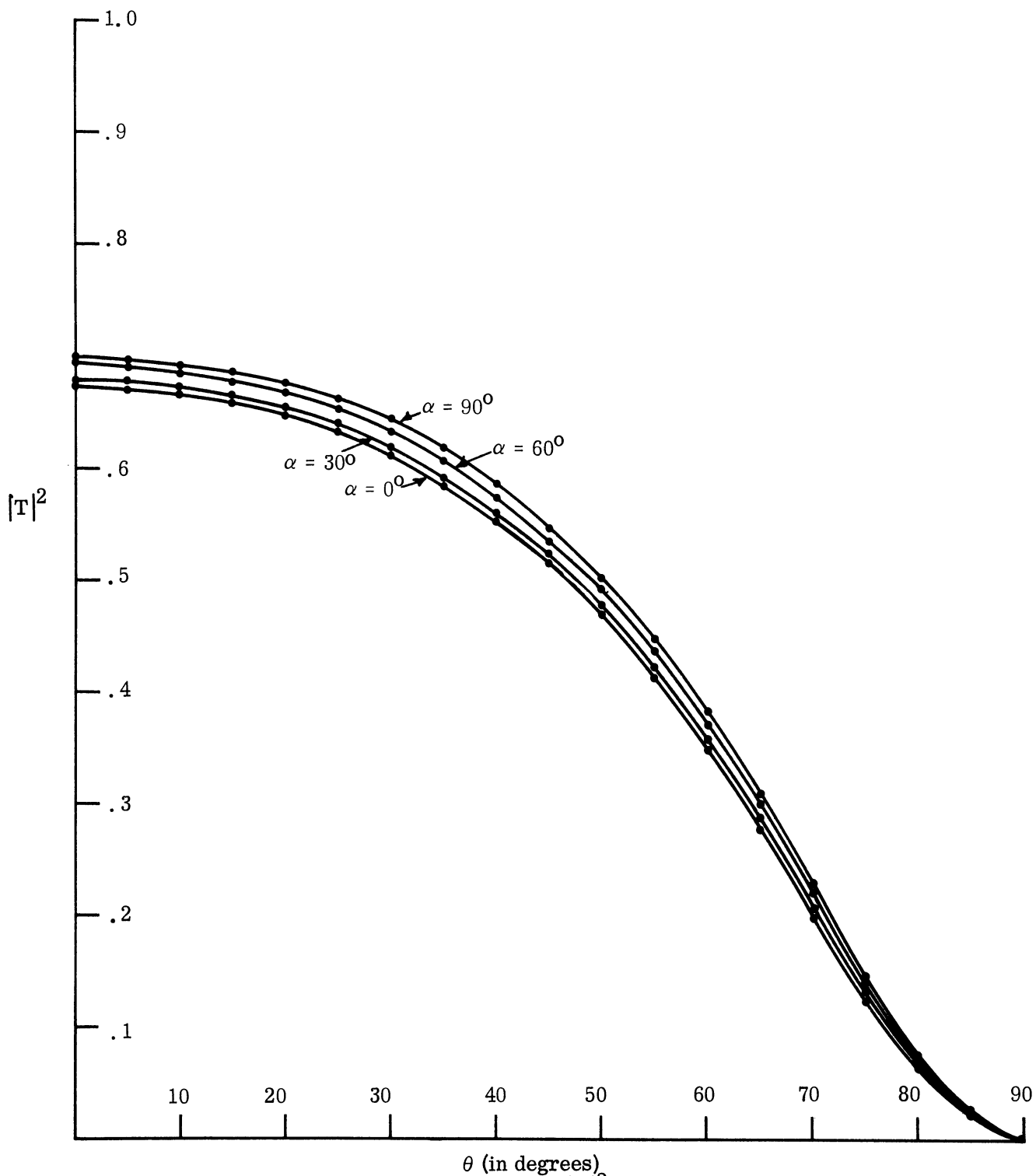


FIG. 3-7: TRANSMISSION COEFFICIENT $|T|^2$ FOR $\epsilon_r=4$, $\epsilon_{1r}=6.6$, $\mu_{1r}=.755$, $(d/\lambda=.04)$.

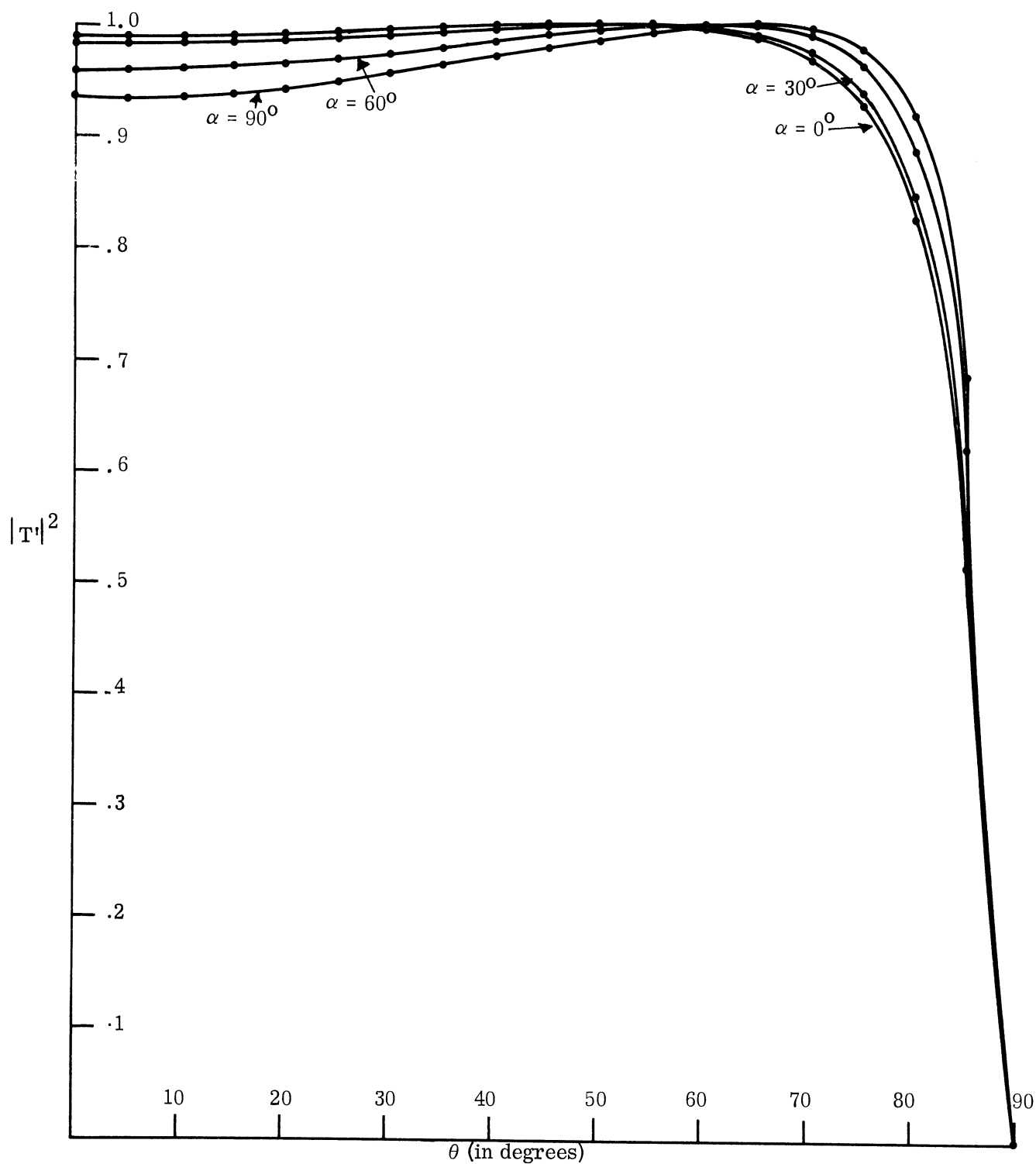


FIG. 3-8: TRANSMISSION COEFFICIENT $|T|^2$ FOR $\epsilon_r=2$, $\epsilon_{1r}=3.3$, $\mu_{1r}=.755$, ($d/\lambda = .04$).

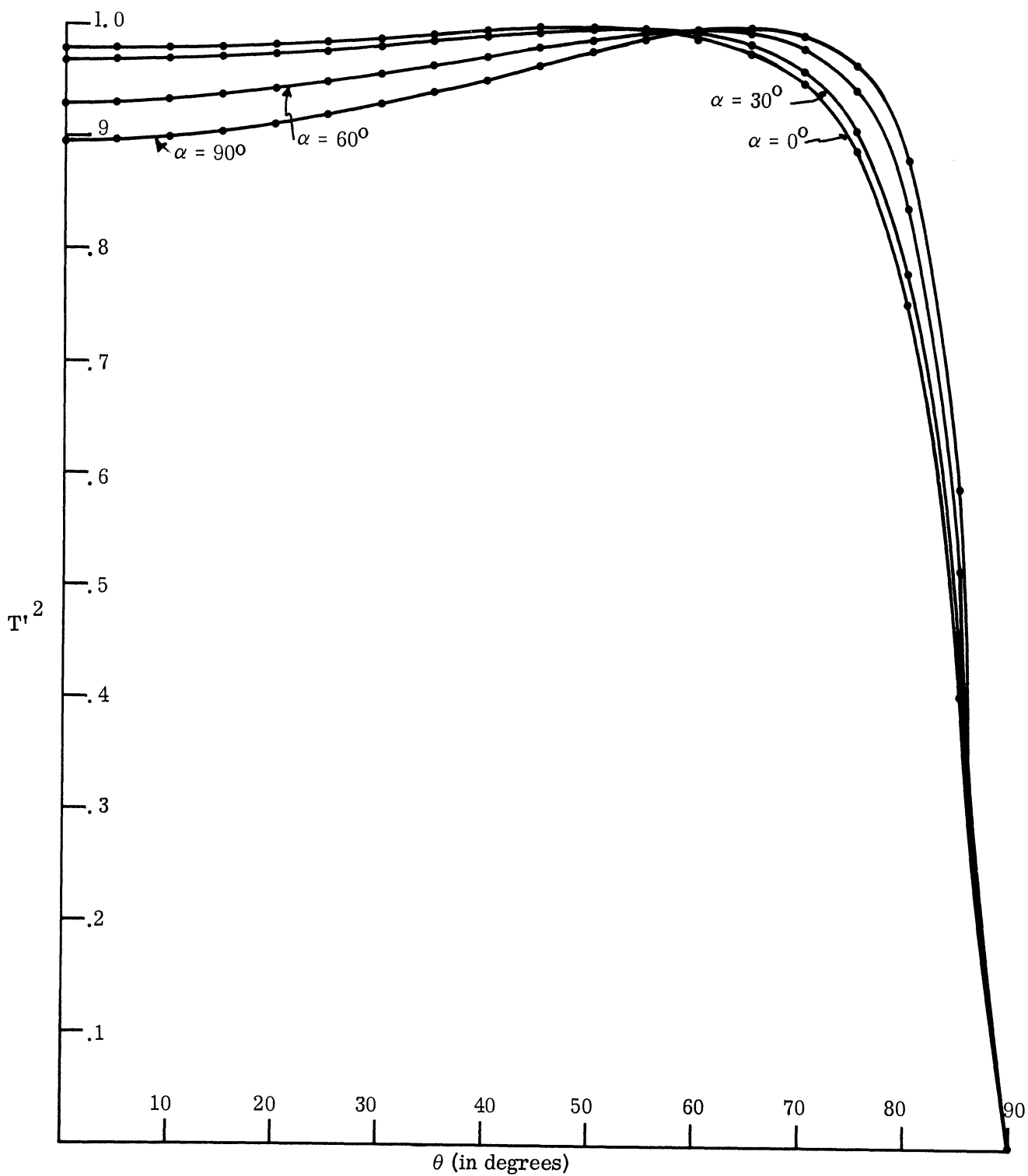


FIG. 3-9: TRANSMISSION COEFFICIENT $|T|^2$ FOR $\epsilon_r=2, \epsilon_{1r}=3.3, \mu_{1r}=.755,$
 $(d/\lambda = .05)$.

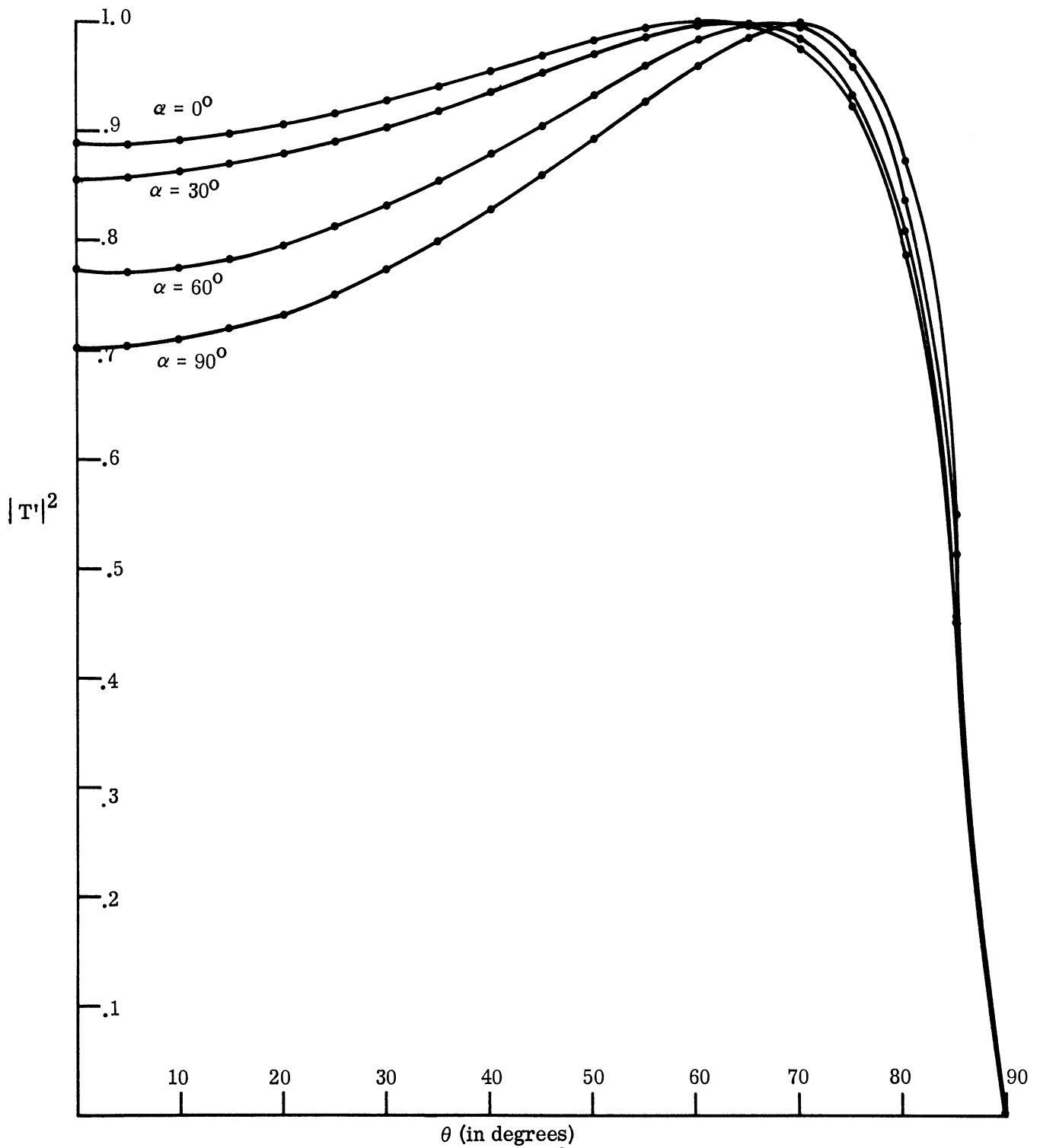


FIG. 3-10: TRANSMISSION COEFFICIENT $|T'|^2$ FOR $\epsilon_r = 4$, $\epsilon_{1r} = 6.6$, $\mu_{1r} = .755$,
 ($d/\lambda = .05$).

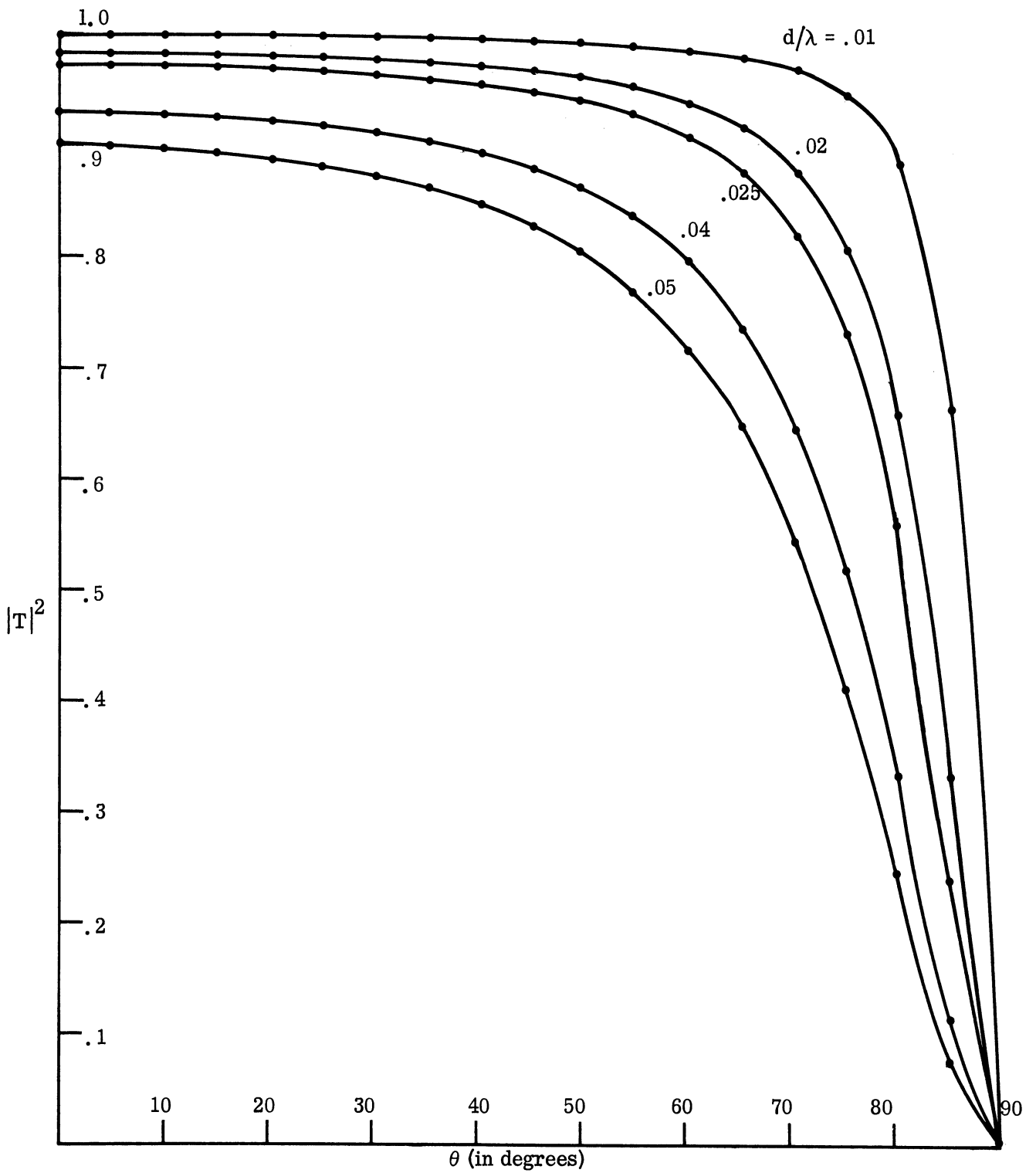


FIG. 3-11: TRANSMISSION COEFFICIENT $|T|^2$ FOR $\epsilon_r=2$, $\epsilon_{1r}=3.3$, $\mu_{1r}=.755$, $\alpha=90^\circ$.

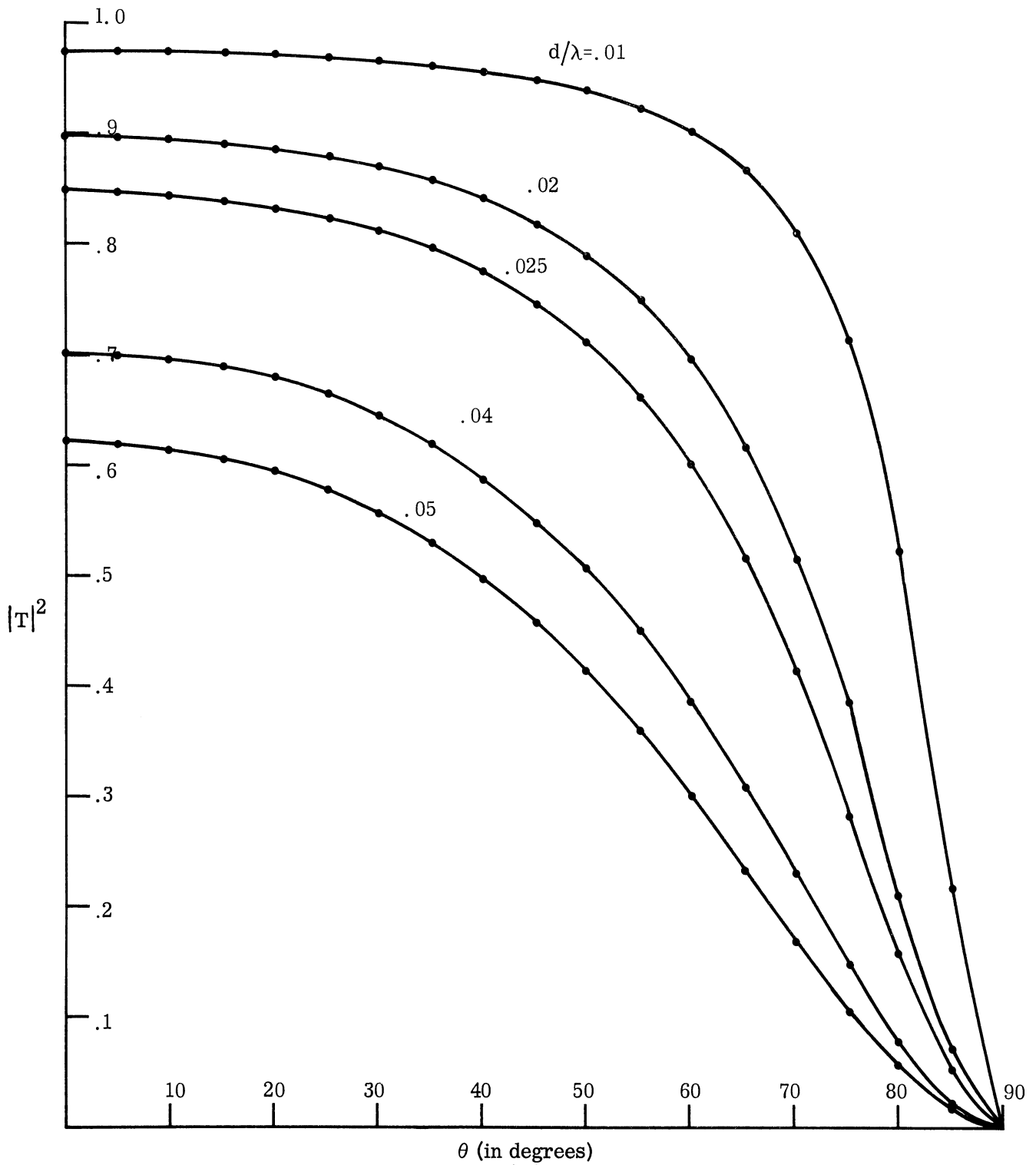


FIG. 3-12: TRANSMISSION COEFFICIENT $|T|^2$ FOR $\epsilon_r=4$, $\epsilon_{1r}=6.6$, $\mu_{1r}=.755$, $\alpha=90^\circ$.

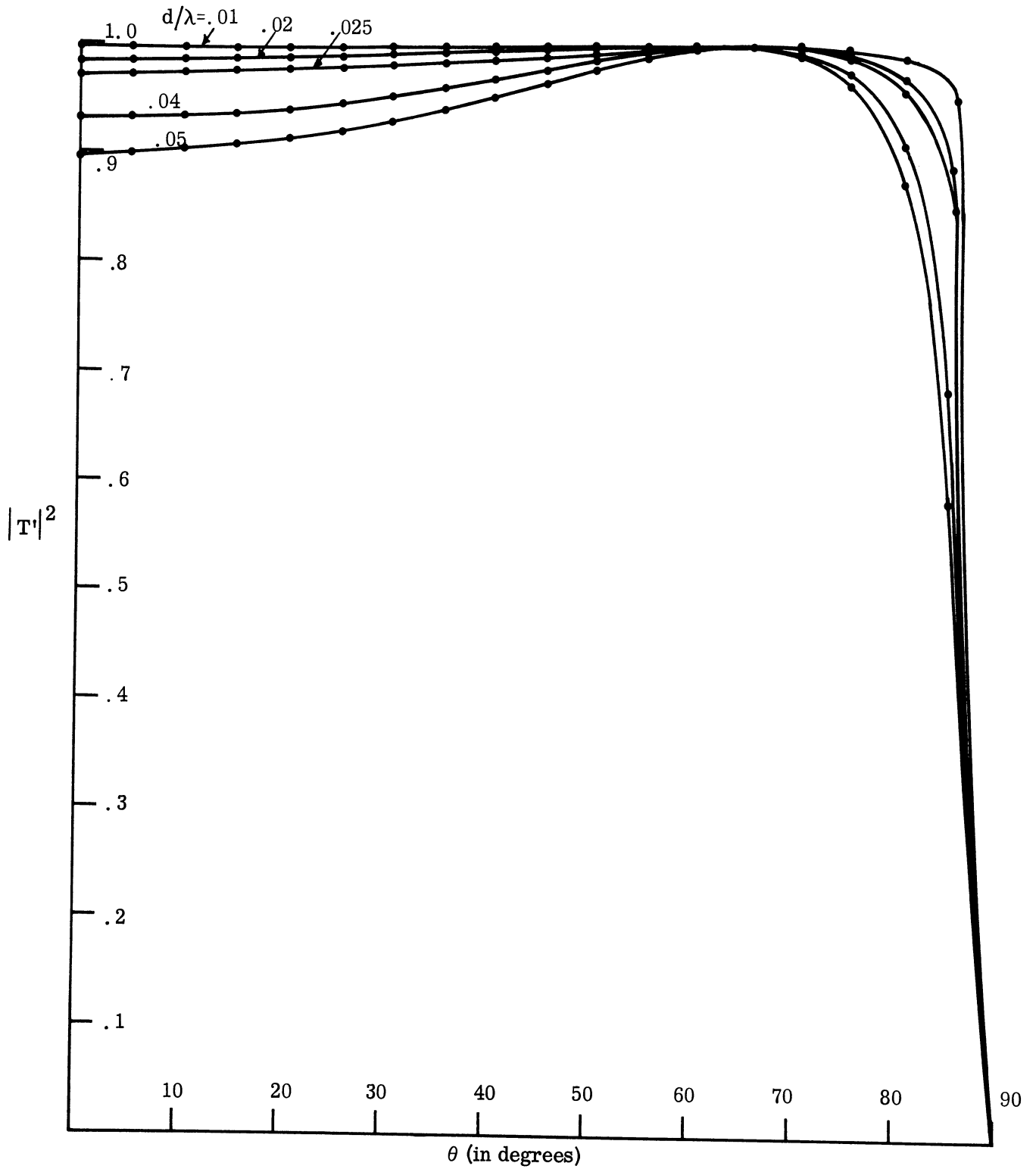


FIG. 3-13: TRANSMISSION COEFFICIENT $|T'|^2$ FOR $\epsilon_r=2$, $\epsilon_{1r}=3.3$, $\mu_{1r}=.755$, $\alpha=90^\circ$.

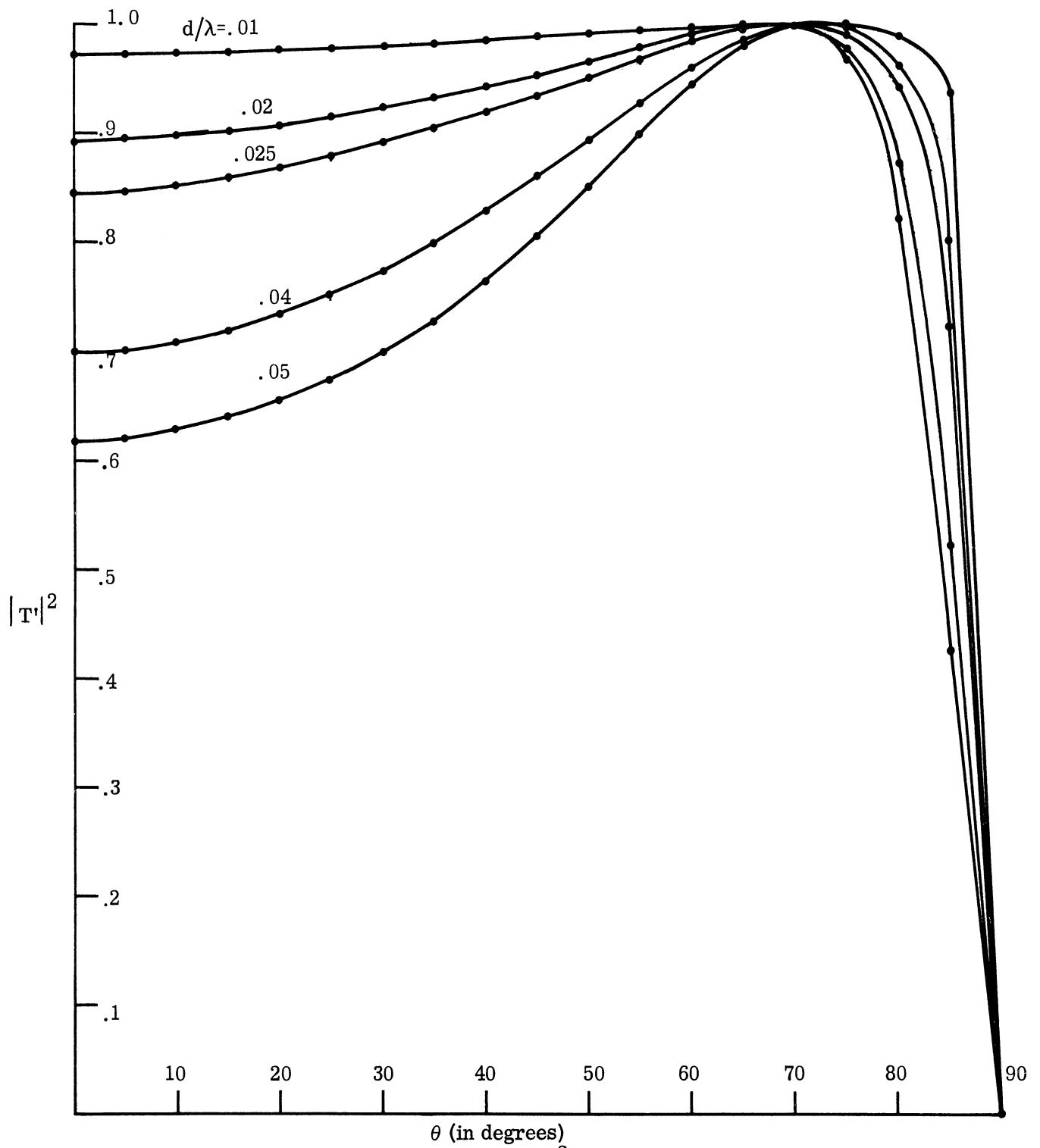


FIG. 3-14: TRANSMISSION COEFFICIENT $|T'|^2$ FOR $\epsilon_r=4$, $\epsilon_{1r}=6.6$, $\mu_{1r}=.755$, $\alpha=90^\circ$.

and $|T'|^2$ becomes unity when

$$\frac{P'd}{\xi_{11}} = N\pi \quad (3.56)$$

Usually $N = 1$ (which corresponds to equivalent half wave panel) is of prime interest. Letting d_t and d'_t represent the corresponding thickness of the panel for which perfect transmission occurs for perpendicular and parallel polarization respectively, it can be shown from the equations (3.55) and (3.56) that

$$d_t = 0.5 \frac{\sqrt{\mu_{1r}} \sin^2 \alpha + \frac{1}{\sqrt{\mu_{1r}}} \cos^2 \alpha}{\sqrt{(\mu_{1r} \sin^2 \alpha + \cos^2 \alpha) \epsilon_{1r} - \sin^2 \theta}} \quad (3.57)$$

$$d'_t = 0.5 \frac{\epsilon_r \sin^2 \alpha + \epsilon_{1r} \cos^2 \alpha}{\sqrt{\epsilon_r \epsilon_{1r}} \sqrt{\epsilon_r \sin^2 \alpha + \epsilon_{1r} \cos^2 \alpha - \sin^2 \theta}} \quad (3.58)$$

These conditions for perfect transmission are plotted in Figs. (3-15) to (3-18). From these plots it is noted that the necessary thicknesses are smallest for $\alpha = \frac{\pi}{2}$, which may be an advantage in some cases where weight is a major factor in a radome design.

In what follows, we discuss the design of an equivalent half wave panel and present the numerical results. The interest is to obtain high transmission for both polarizations for all angles of incidence up to 85° .

As noted before, perfect transmission is obtained for parallel polarization when the incident angle θ is equal to the Brewster angle θ_B . It was also noted that θ_B has maximum value, and better transmission is obtained for perpendicular polarization

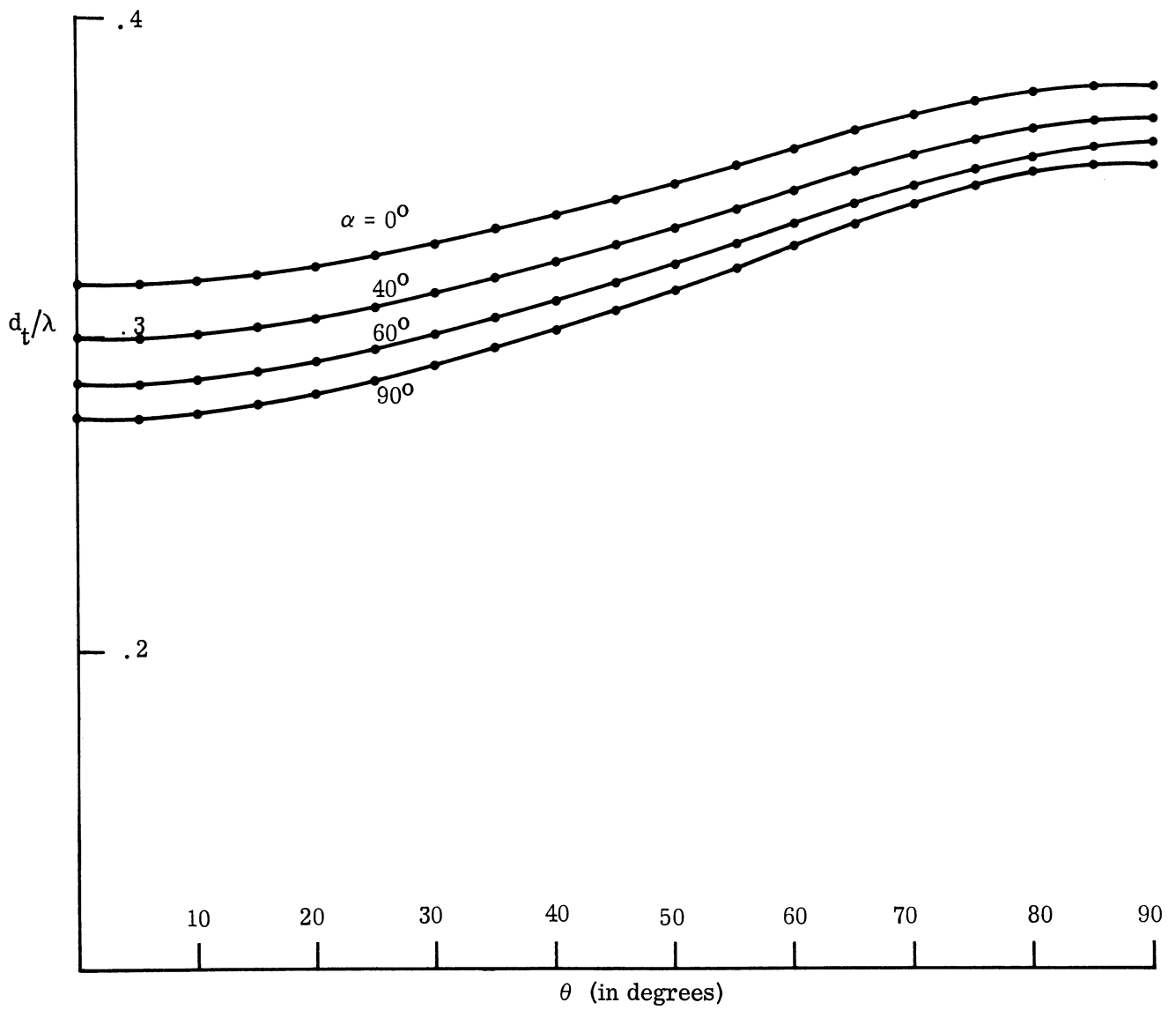


FIG. 3-15: CONDITIONS FOR PERFECT TRANSMISSION ($|T|^2=1$) THROUGH EQUIVALENT HALF-WAVE PANEL FOR $\epsilon_r=2$, $\epsilon_{1r}=3.3$, $\mu_{1r}=.755$.

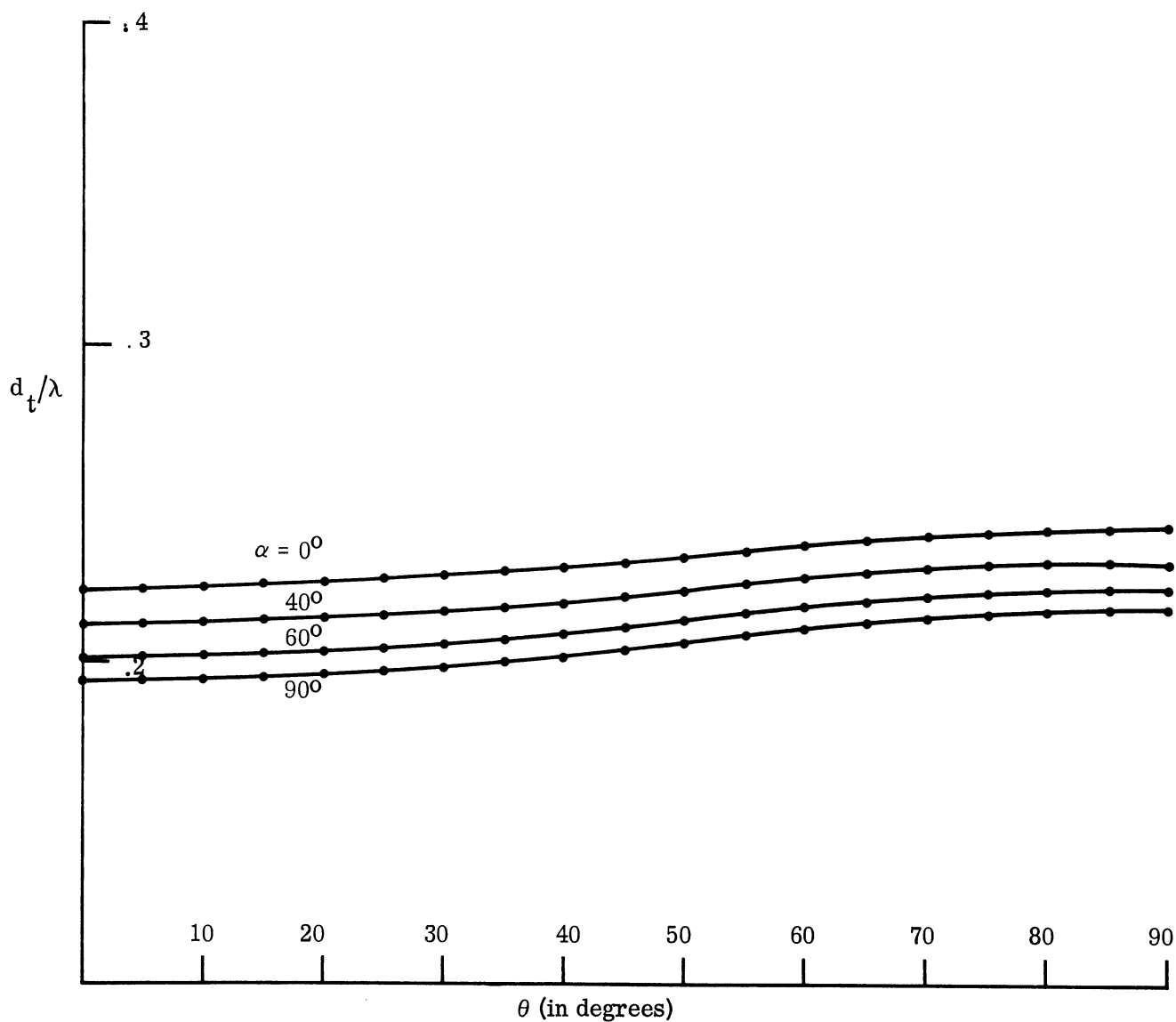


FIG. 3-16: CONDITIONS FOR PERFECT TRANSMISSION ($|T|^2=1$) THROUGH AN EQUIVALENT HALF-WAVE PANEL FOR $\epsilon_r=4$, $\epsilon_{1r}=6.6$, $\mu_{1r}=.755$.

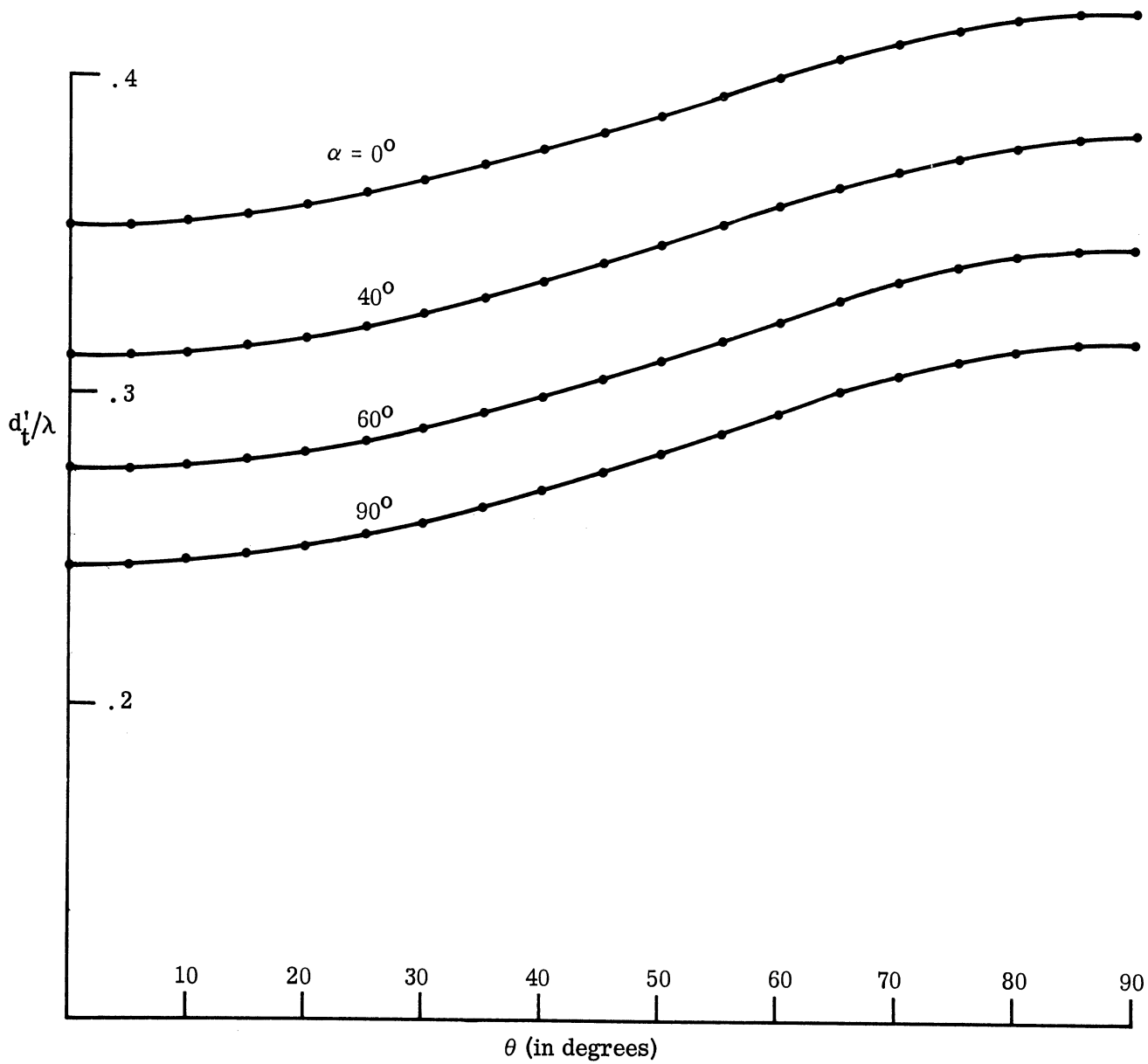


FIG. 3-17: CONDITIONS FOR PERFECT TRANSMISSION ($|T|^2=1$) THROUGH AN EQUIVALENT HALF-WAVE PANEL FOR $\epsilon_r=2$, $\epsilon_{1r}=3.3$, $\mu_{1r}=.755$.

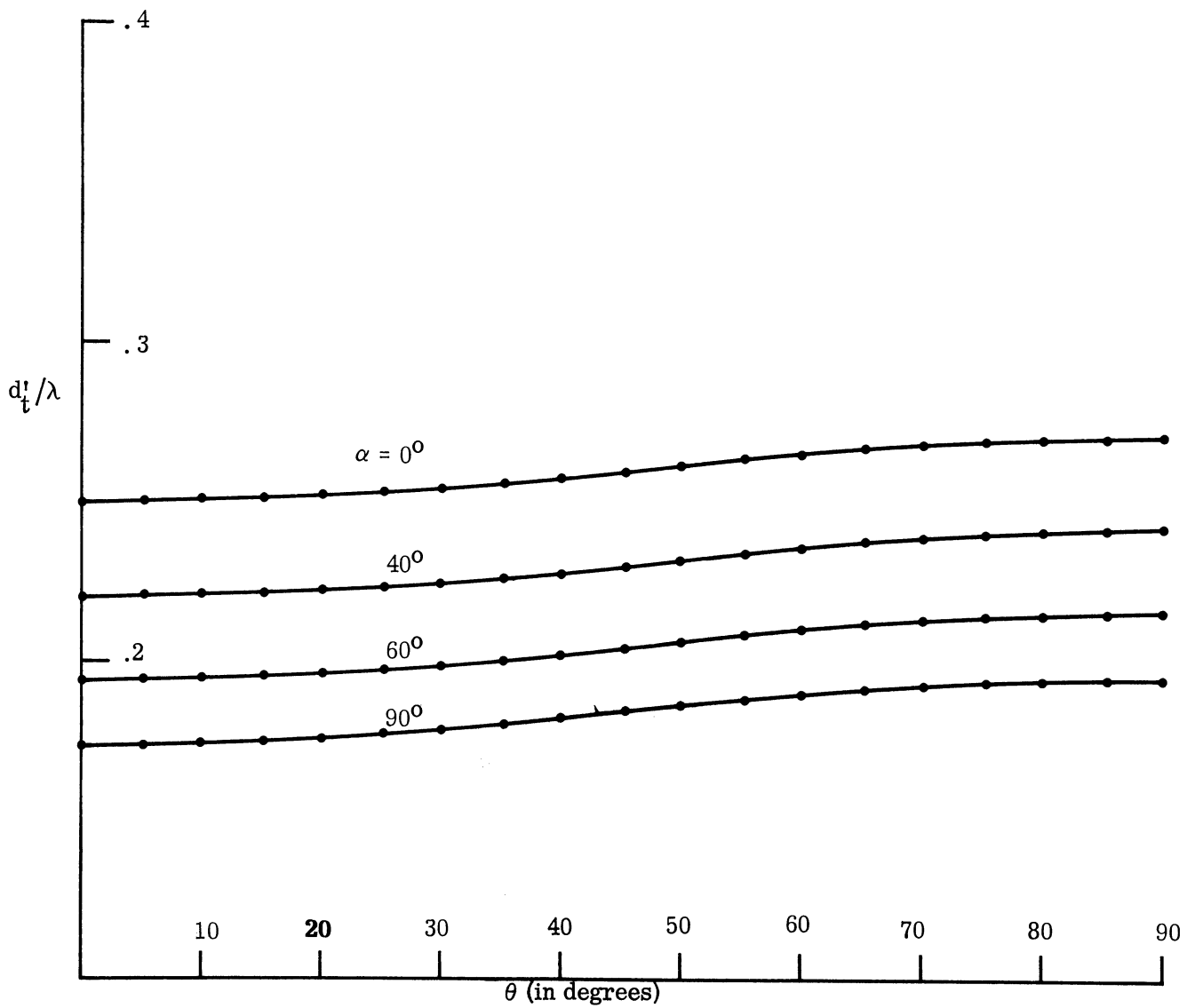


FIG. 3-18: CONDITIONS FOR PERFECT TRANSMISSION ($|T'|^2=1$) THROUGH AN EQUIVALENT HALF-WAVE PANEL FOR $\epsilon_r=4$, $\epsilon_{1r}=6.6$, $\mu_{1r}=.755$.

when $\alpha = \frac{\pi}{2}$. Considering these observations, it is appropriate to design the equivalent half wave panel in such a way that perfect transmission is obtained for perpendicular polarization at a desired angle θ_t , which is related to the required thickness d_t as given in equation (3.57) for $\alpha = \frac{\pi}{2}$. Figures 3-19 to 3-24 represent the transmission coefficient $|T|^2$ as a function of θ and α for several assumed values of θ_t . Similarly, Figs. 3-25 to 3-30 represent $|T'|^2$. Figures 3-31 to 3-34 represent $|T|^2$ or $|T'|^2$ as a function of θ and θ_t for $\alpha = \frac{\pi}{2}$. From these figures it is noted that higher the value of θ_t , the better is the transmission at high incident angles, for the case of $\alpha = \frac{\pi}{2}$. However as θ_t is increased to higher values, the transmission efficiency at normal incidence is degraded for $\alpha = \frac{\pi}{2}$. For $\alpha < \frac{\pi}{2}$, the transmission efficiency is better for normal incidence. This dependence of the transmission coefficients on α can be taken as an advantage in order to obtain high transmission throughout the range of incident angles. We take the case of $\epsilon_r = 4$, $\epsilon_{1r} = 6.6$, and $\theta_t = 80^\circ$, as it has the better transmission for high incident angles (up to $\theta = 85^\circ$) for $\alpha = \frac{\pi}{2}$, to illustrate how one could design a panel which has power transmission efficiencies better than 95 per cent over the range of incident angles up to $\theta = 85^\circ$. To do this, draw a line at $|T|^2 = .95$ (and $|T'|^2 = .95$) in Fig. 3-24 (and Fig. 3-30). From these figures, it is noted that the curves for $\alpha = 30^\circ$ can be used up to $\theta = 35^\circ$, $\alpha = 60^\circ$ can be used from 35° to 65° and $\alpha = 90^\circ$ can be used for higher values of θ . To apply these results to a cone shaped radome, one has to vary α along the radome depending on the angle of incidence as shown in Fig. 3-35.

The corresponding transmission coefficients are plotted in Fig. 3-36. It is expected that by varying α continuously along the radome the transmission efficiencies could be improved further.

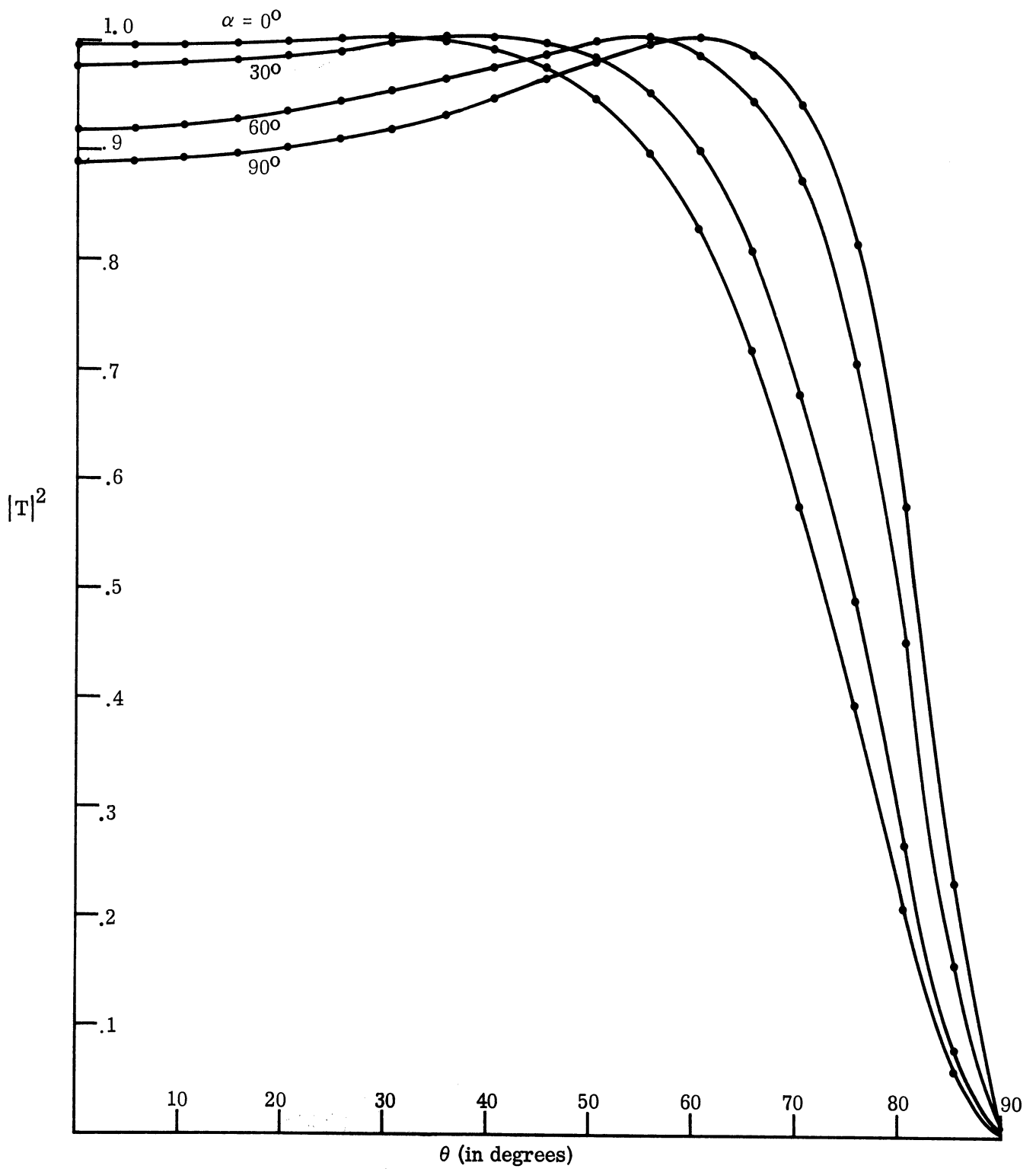


FIG. 3-19: TRANSMISSION COEFFICIENT $|T|^2$ FOR $\theta_t=60^\circ$ ($d_t/\lambda=.329$), $\epsilon_r=2$, $\epsilon_{1r}=3.3$, $\mu_{1r}=.755$.

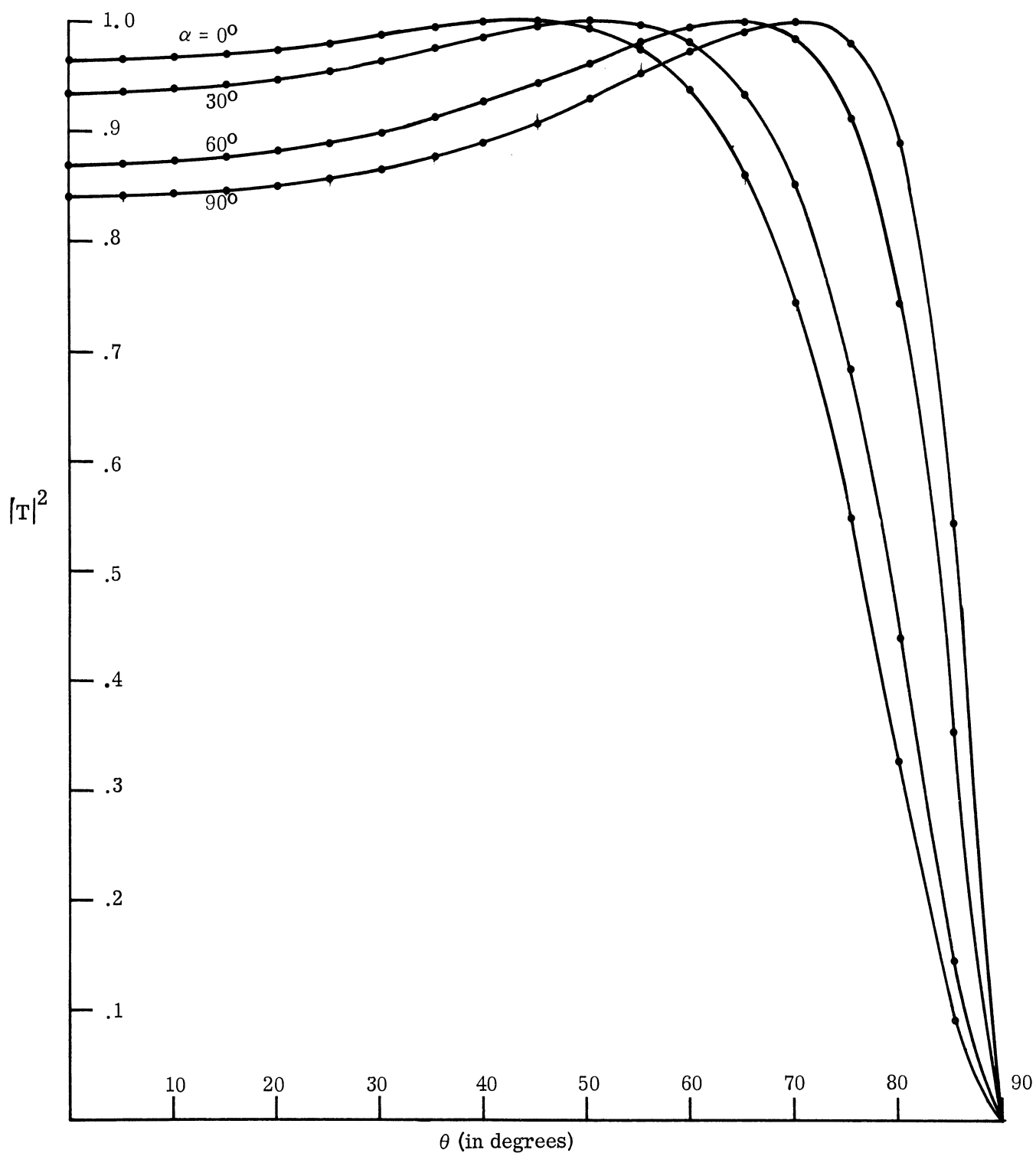


FIG. 3-20: TRANSMISSION COEFFICIENT $|T|^2$ FOR $\theta_t = 70^\circ$ ($d_t/\lambda = .342$), $\epsilon_r = 2$, $\epsilon_{1r} = 3.3$, $\mu_{1r} = .755$.

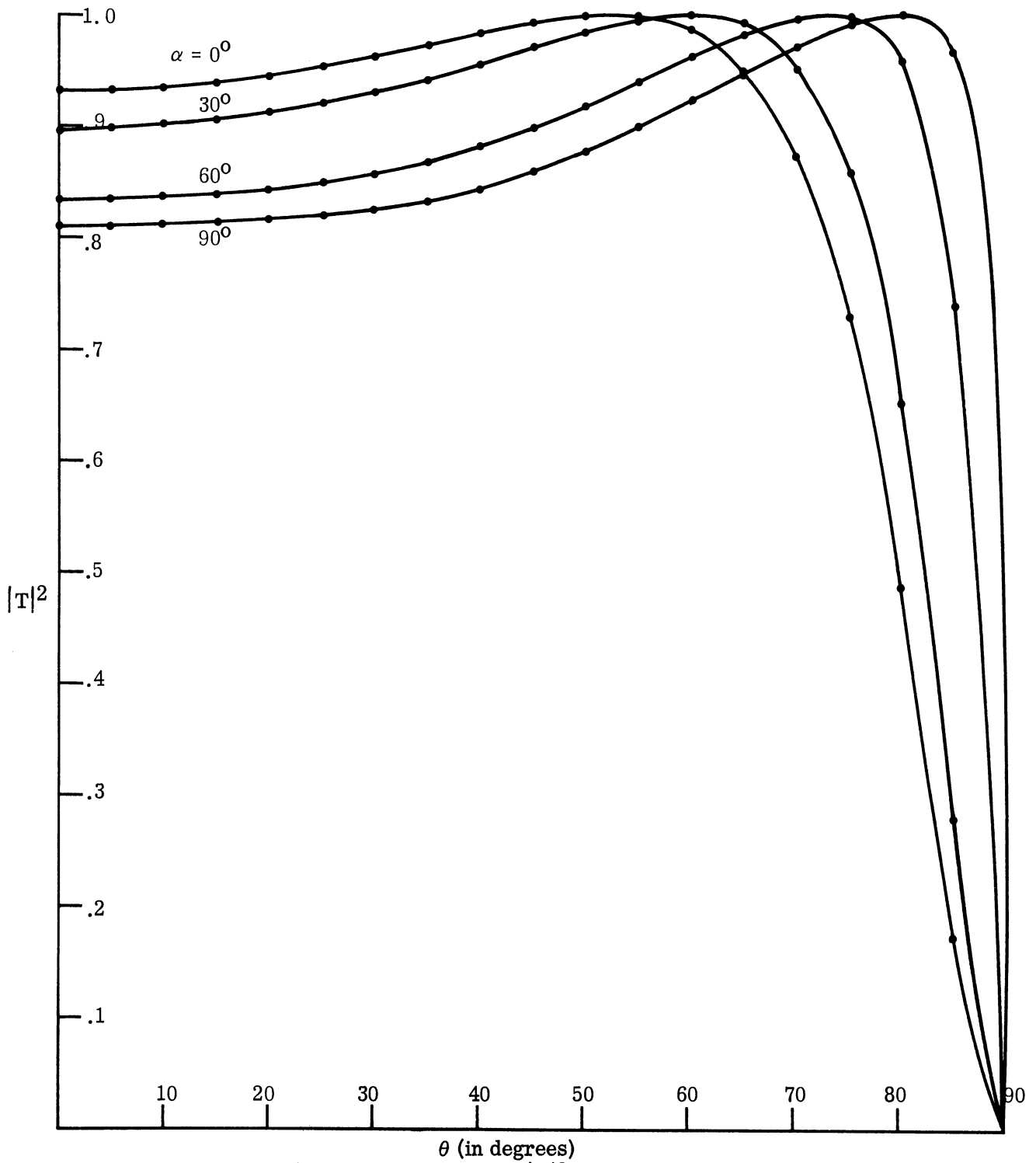


FIG. 3-21: TRANSMISSION COEFFICIENT $|T|^2$ FOR $\theta_t=80^\circ$ ($d_t/\lambda = .352$), $\epsilon_r=2$, $\epsilon_{1r} = 3.3$, $\mu_{1r} = .755$.

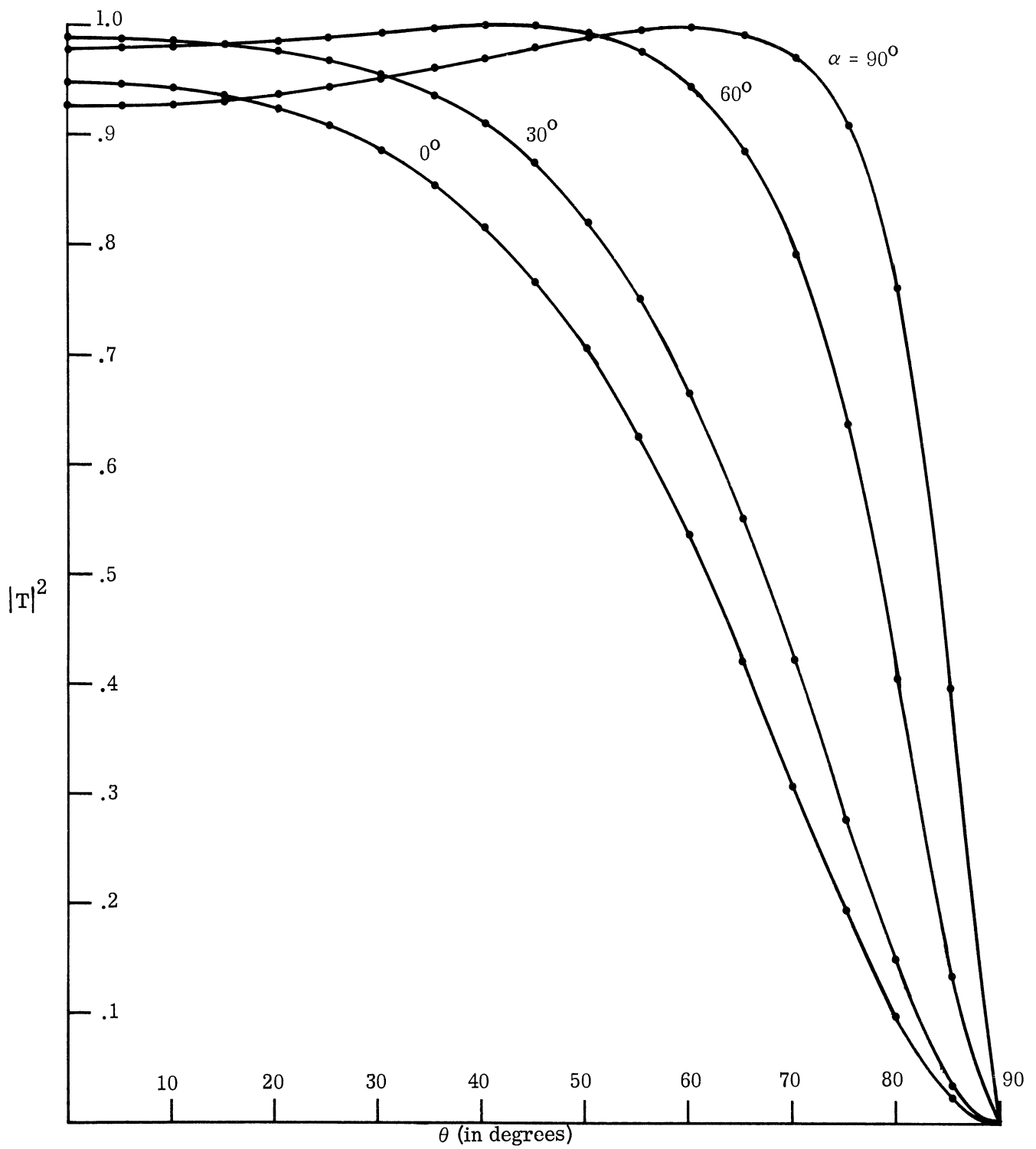


FIG. 3-22: TRANSMISSION COEFFICIENT $|T|^2$ FOR $\theta_t=60^\circ$ ($d_t/\lambda=.211$), $\epsilon_r=4$, $\epsilon_{1r}=6.6$, $\mu_{1r}=.755$.

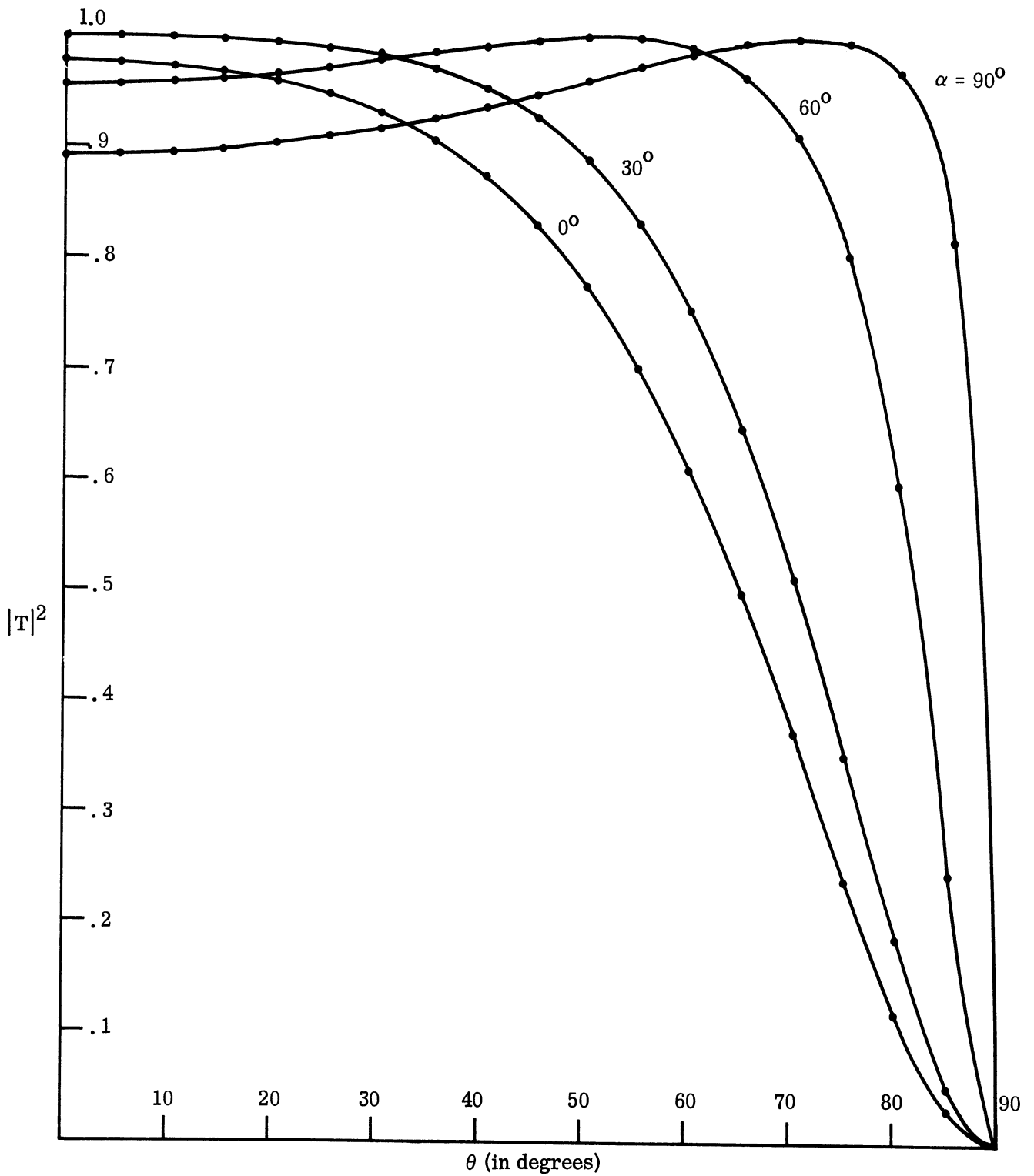


FIG. 3-23: TRANSMISSION COEFFICIENT $|T|^2$ FOR $\theta_t = 70^\circ$ ($d_t/\lambda = .215$), $\epsilon_r = 4$, $\epsilon_{1r} = 6.6$, $\mu_{1r} = .755$.

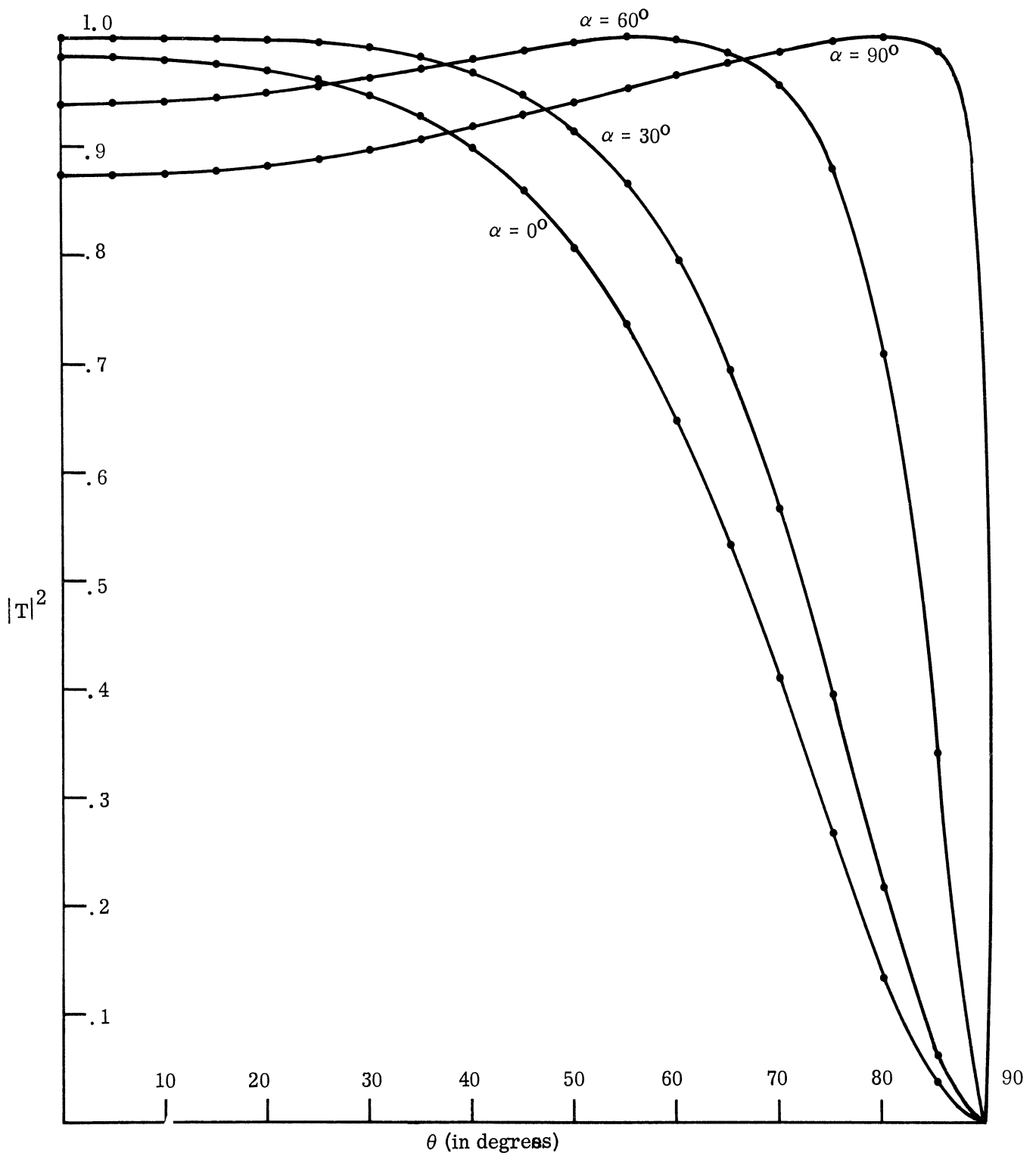


FIG. 3-24: TRANSMISSION COEFFICIENT $|T|^2$ FOR $\theta_t=80^\circ$ ($d_t/\lambda=.217$), $\epsilon_r=4$, $\epsilon_{1r}=6.6$, $\mu_{1r}=.755$.

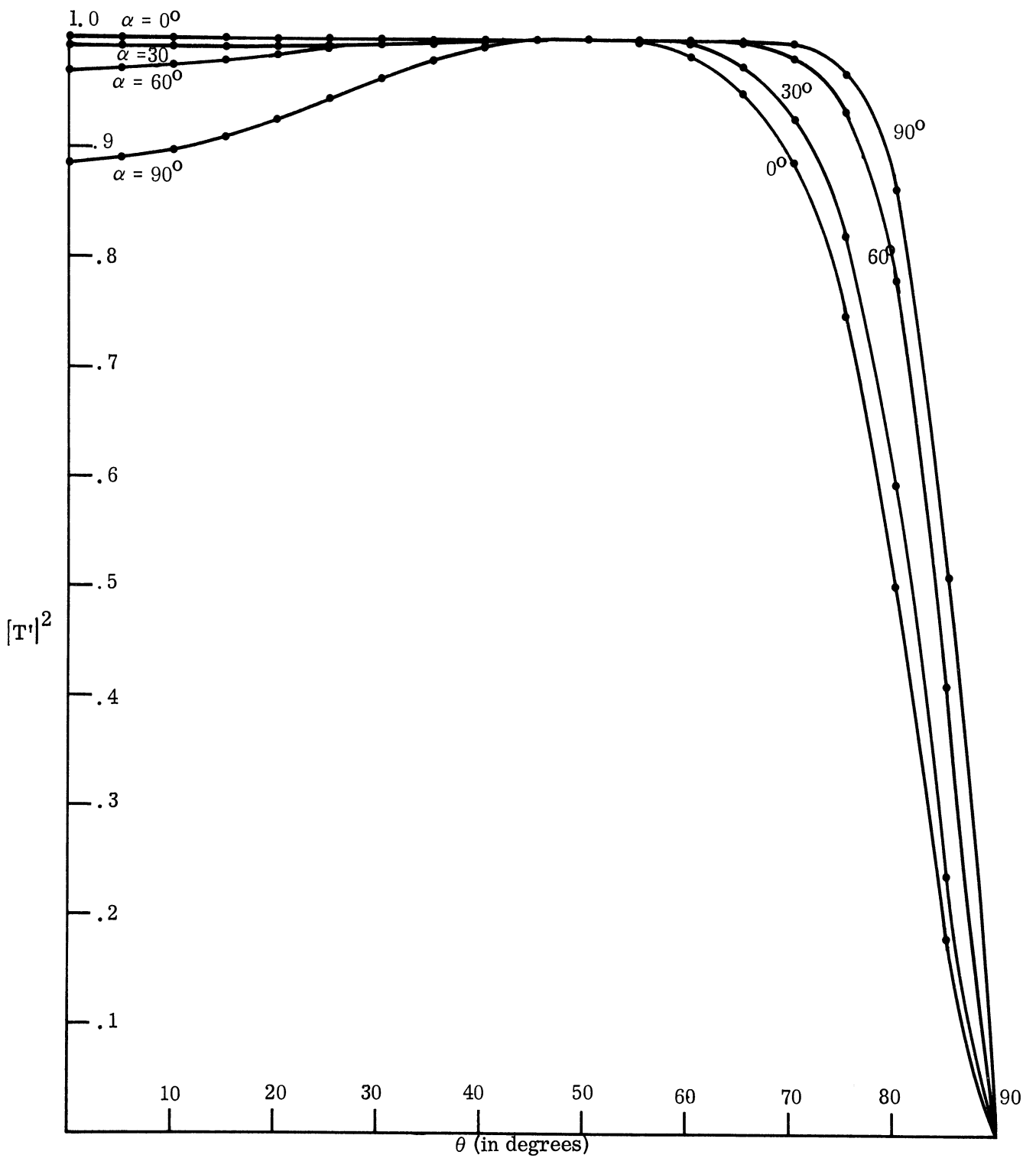


FIG. 3-25: TRANSMISSION COEFFICIENT $|T'|^2$ FOR $\theta_t = 60^\circ (d_t/\lambda = .329)$, $\epsilon_r = 2$, $\epsilon_{1r} = 3.3$, $\mu_{1r} = .755$

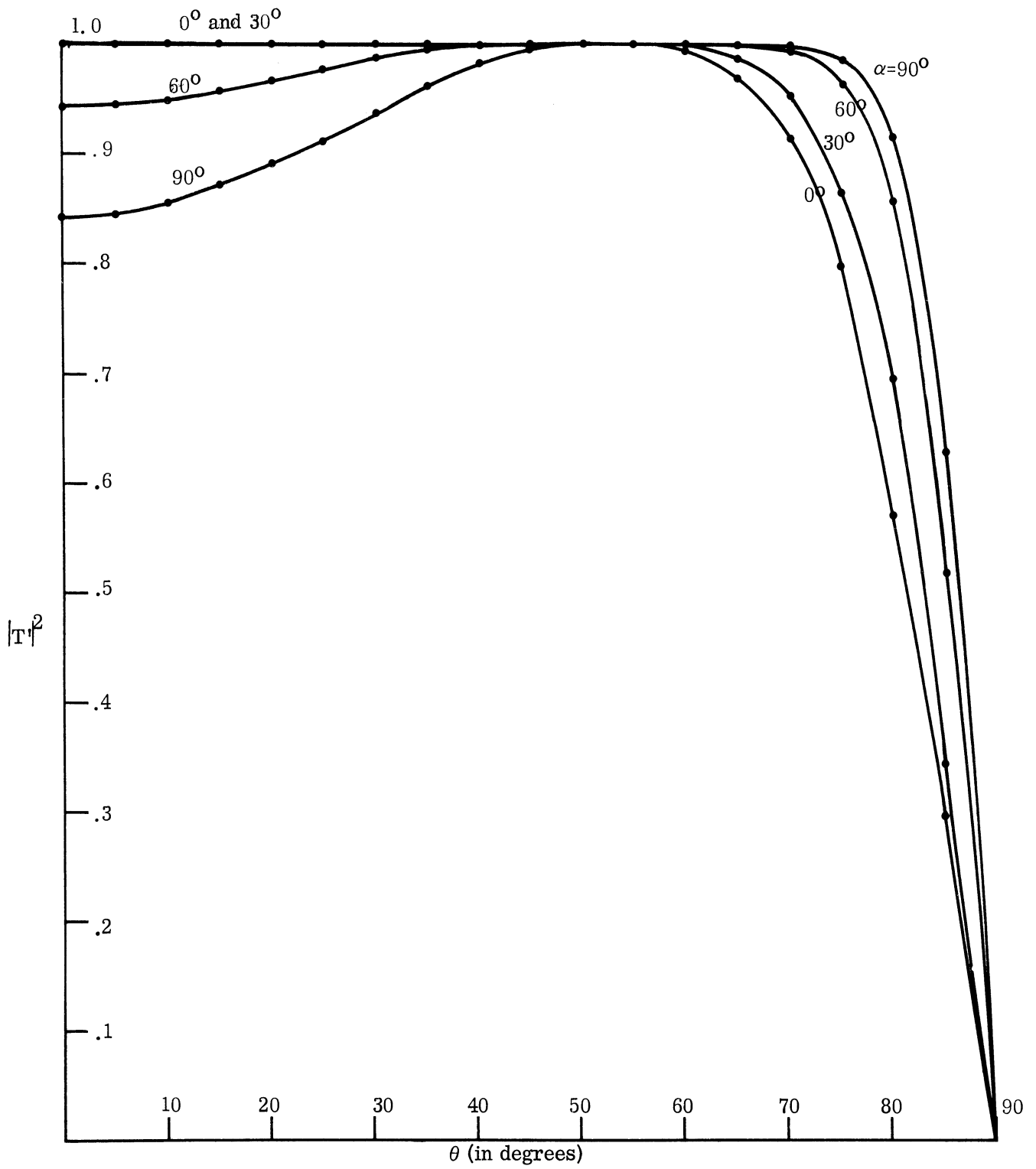


FIG. 3-26: TRANSMISSION COEFFICIENT $|T|^2$ FOR $\theta_t = 70^\circ$ ($d_t/\lambda = .342$) $\epsilon_r = 2$, $\epsilon_{1r} = 3.3$, $\mu_{1r} = .755$.

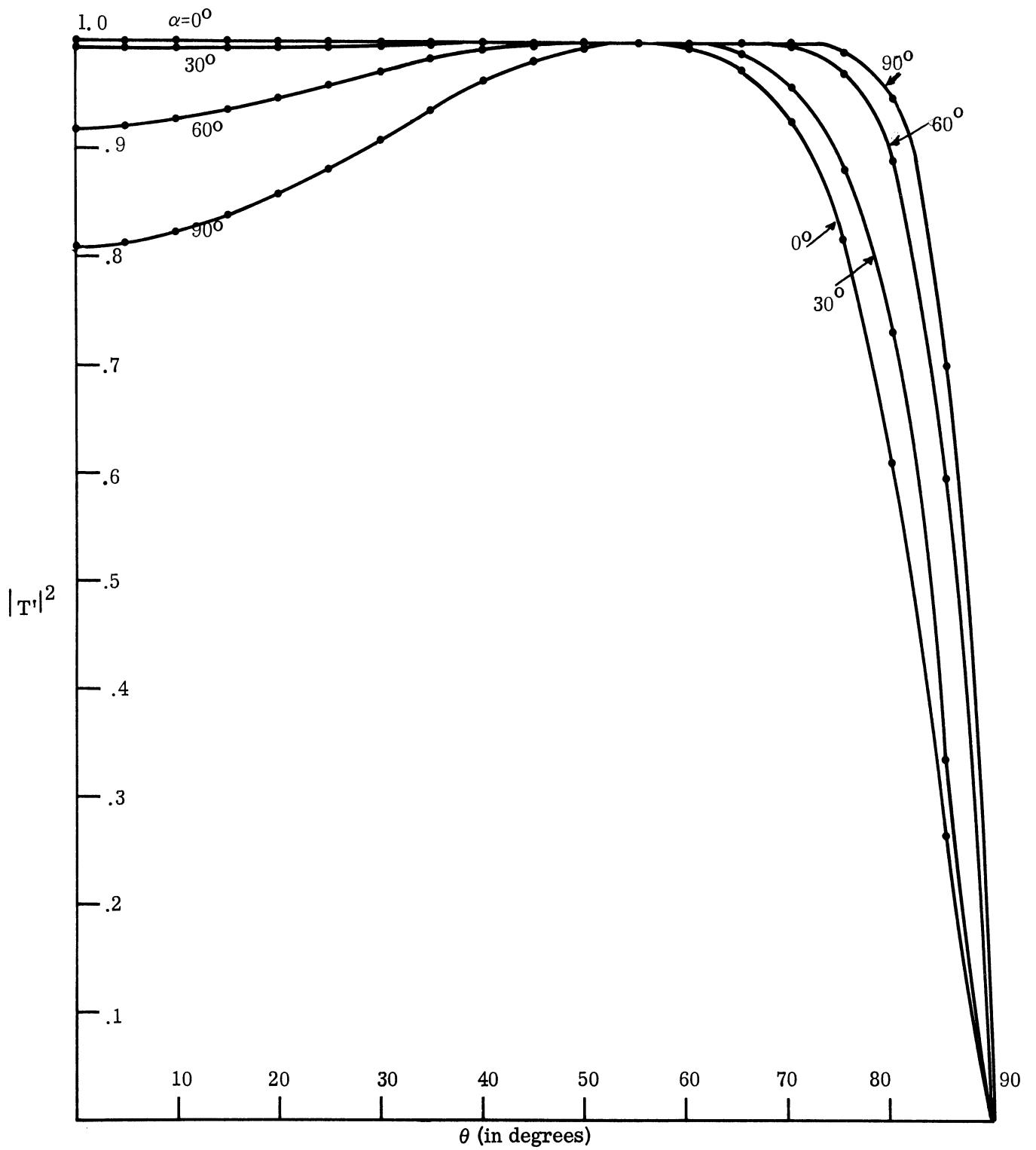


FIG. 3-27: TRANSMISSION COEFFICIENT $|T'|^2$ FOR $\theta_t=80^\circ$ ($d_t/\lambda = .352$), $\epsilon_r=2$, $\epsilon_{1r}=3.3$, $\mu_{1r}=.755$.

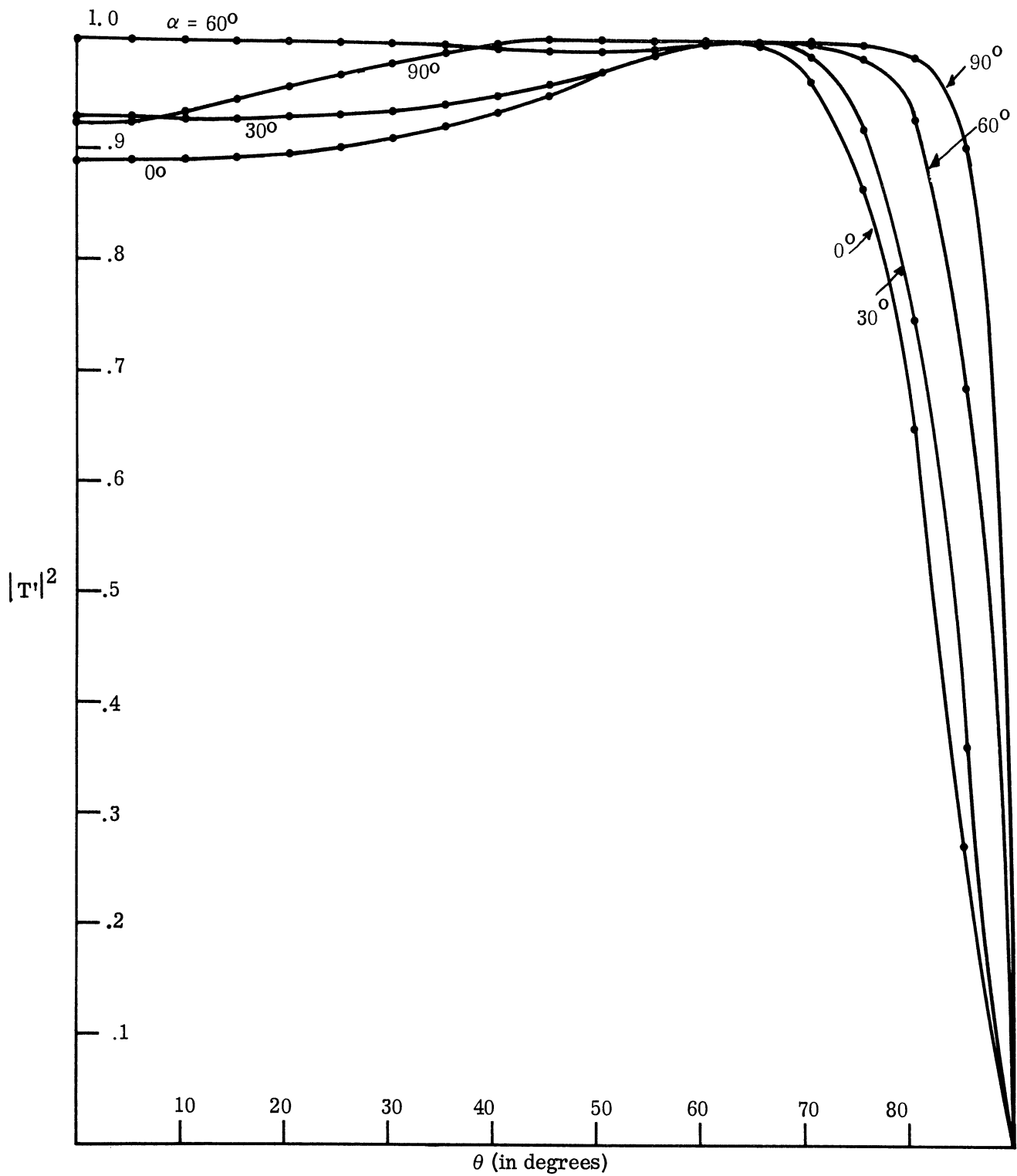


FIG. 3-28: TRANSMISSION COEFFICIENT $|T|^2$ FOR $\theta_t = 60^\circ$ ($d_t/\lambda = .211$), $\epsilon_r = 4$, $\epsilon_{1r} = 6.6$, $\mu_{1r} = .755$.

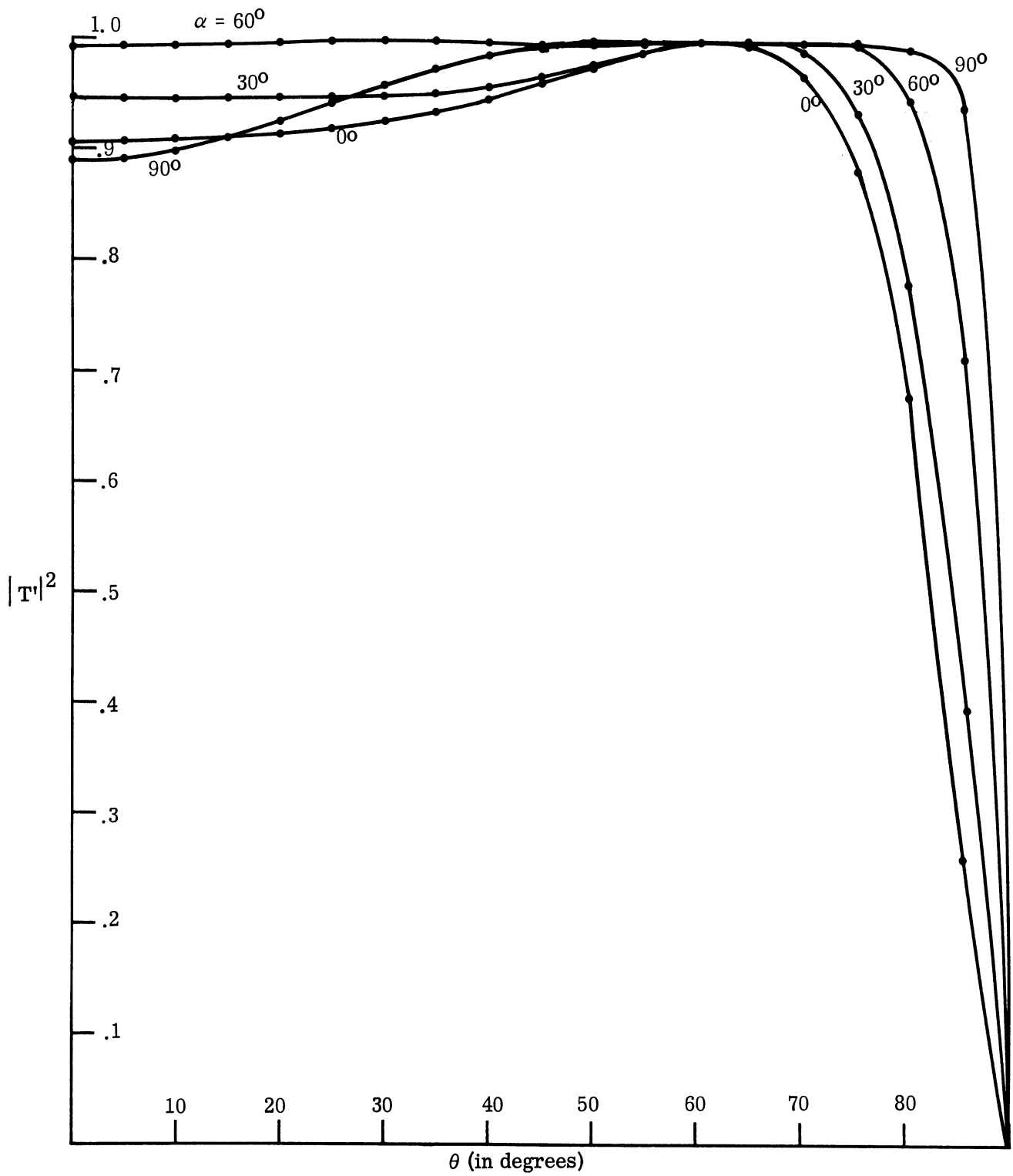


FIG. 3-29: TRANSMISSION COEFFICIENT $|T'|^2$ FOR $\theta_t = 70^\circ$ ($d_t/\lambda = .215$), $\epsilon_r = 4$, $\epsilon_{1r} = 6.6$, $\mu_{1r} = .755$.

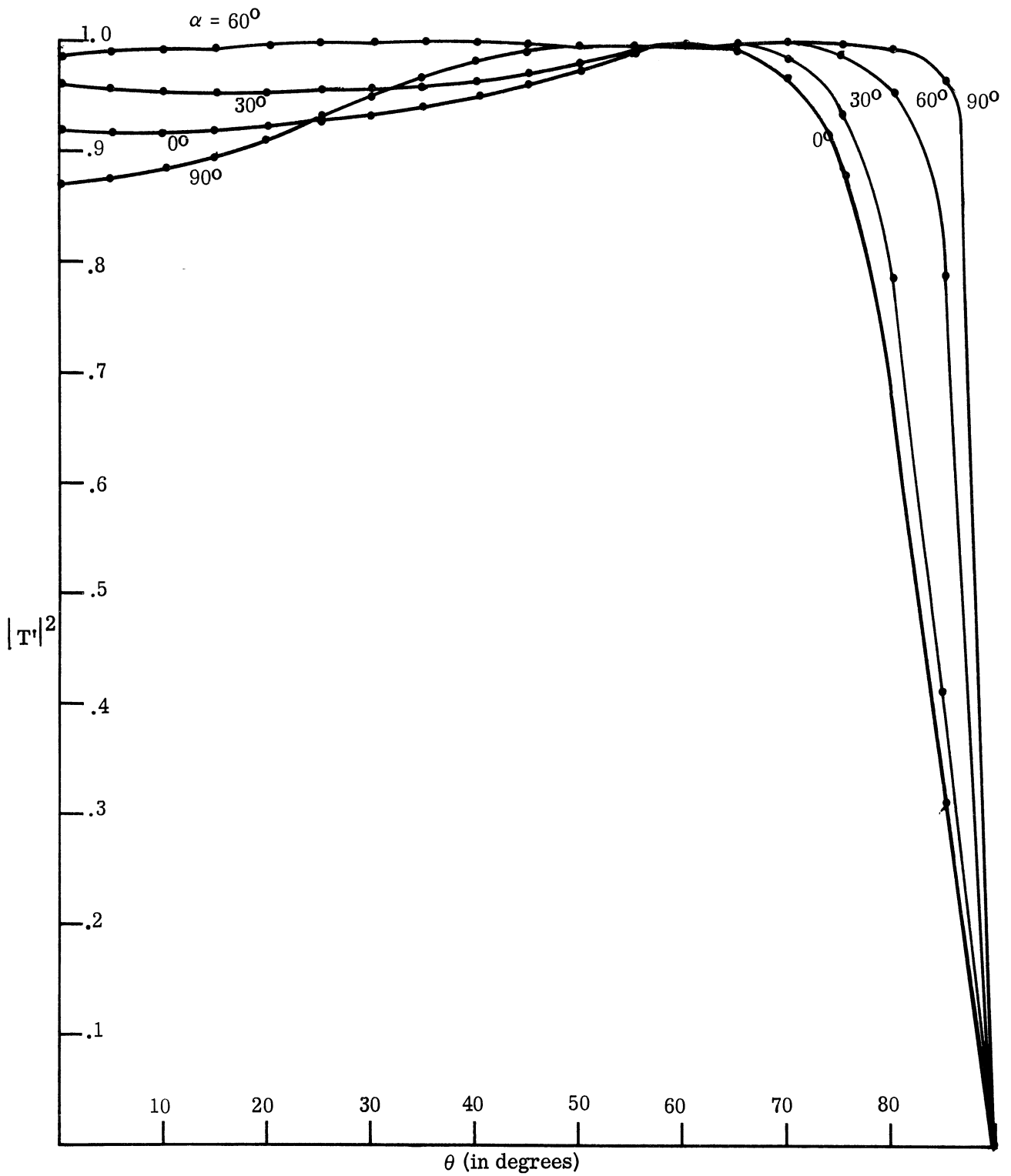


FIG. - 3-30: TRANSMISSION COEFFICIENT $|T|^2$ FOR $\theta_t=80^\circ(d_t/\lambda=.217)$, $\epsilon_r=4$, $\epsilon_{1r}=6.6$, $\mu_{1r}=.755$.

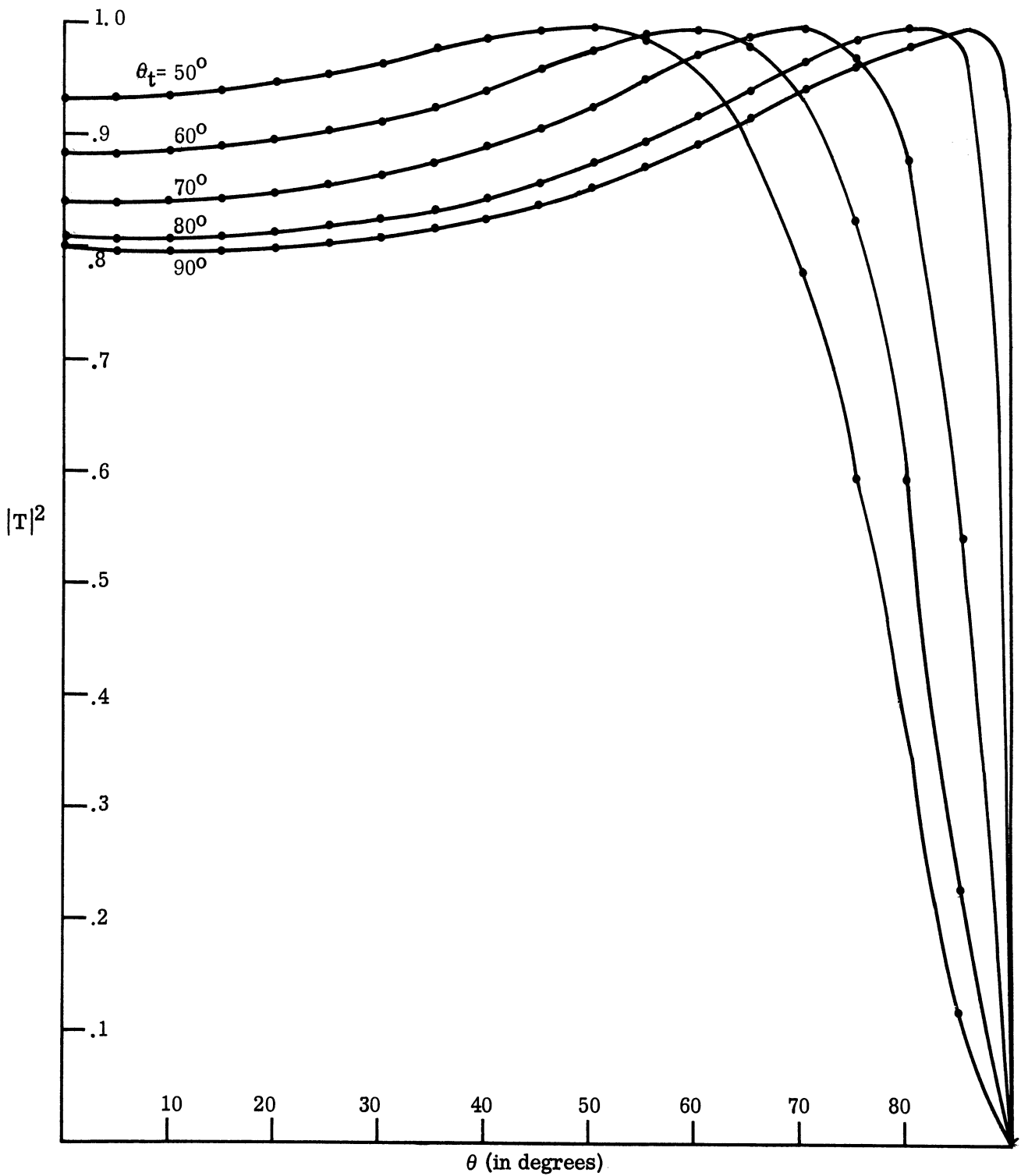


FIG. 3-31: TRANSMISSION COEFFICIENT $|T|^2$ FOR $\epsilon_r=2$, $\epsilon_{1r}=3.3$, $\mu_{1r}=.755$, $\alpha = 90^\circ$ AND VARIOUS VALUES OF θ_t .

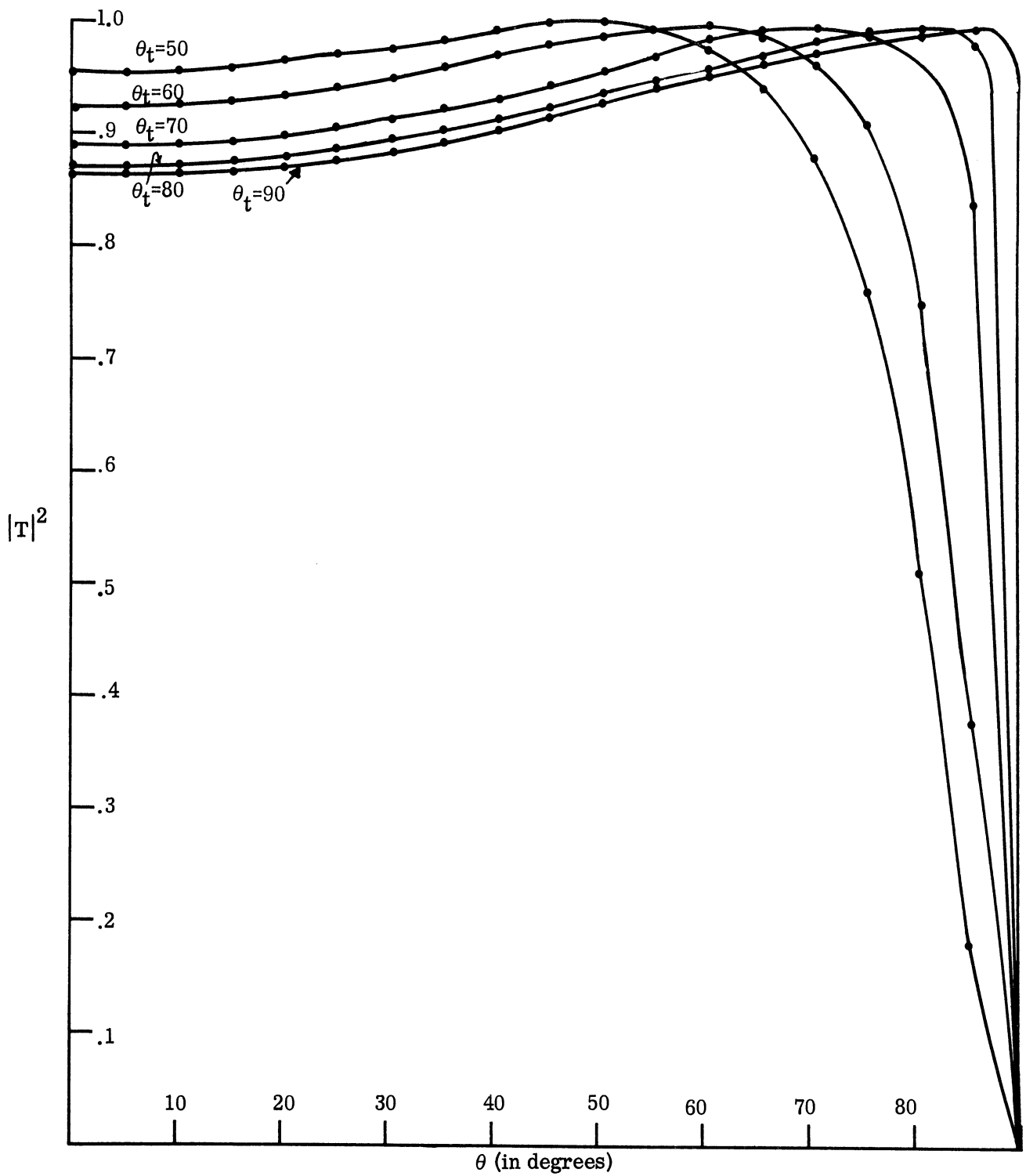


FIG. 3-32: TRANSMISSION COEFFICIENT $|T|^2$ FOR $\epsilon_r = 4$, $\epsilon_{1r} = 6.6$, $\mu_{1r} = .755$
 $\alpha = 90^\circ$ AND VARIOUS VALUES OF θ_t .

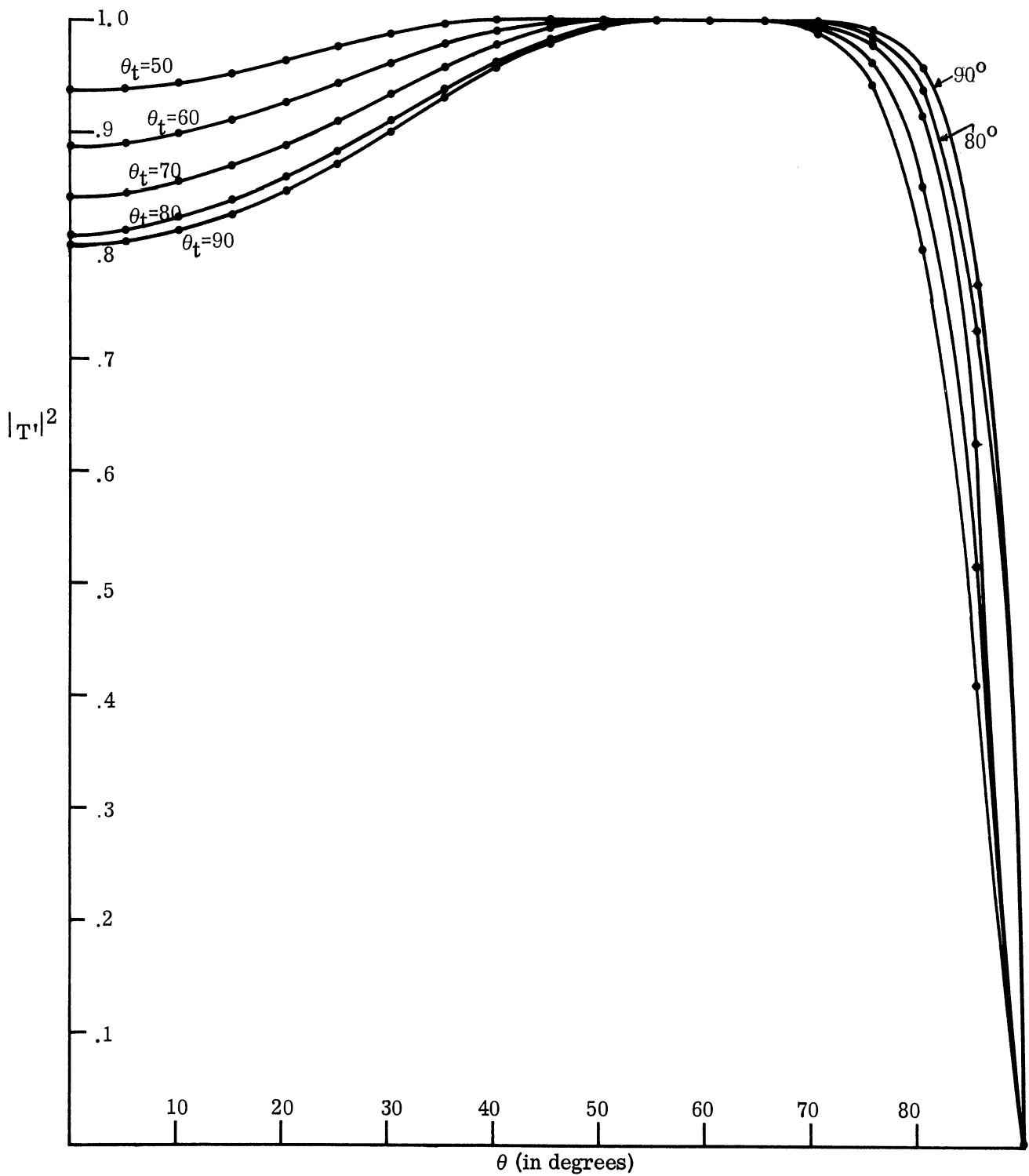


FIG. 3-33: TRANSMISSION COEFFICIENT $|T|^2$ FOR $\epsilon_r=2$, $\epsilon_{1r}=3.3$, $\mu_{1r} = .755$, $\alpha = 90^\circ$ AND VARIOUS VALUES OF θ_t .

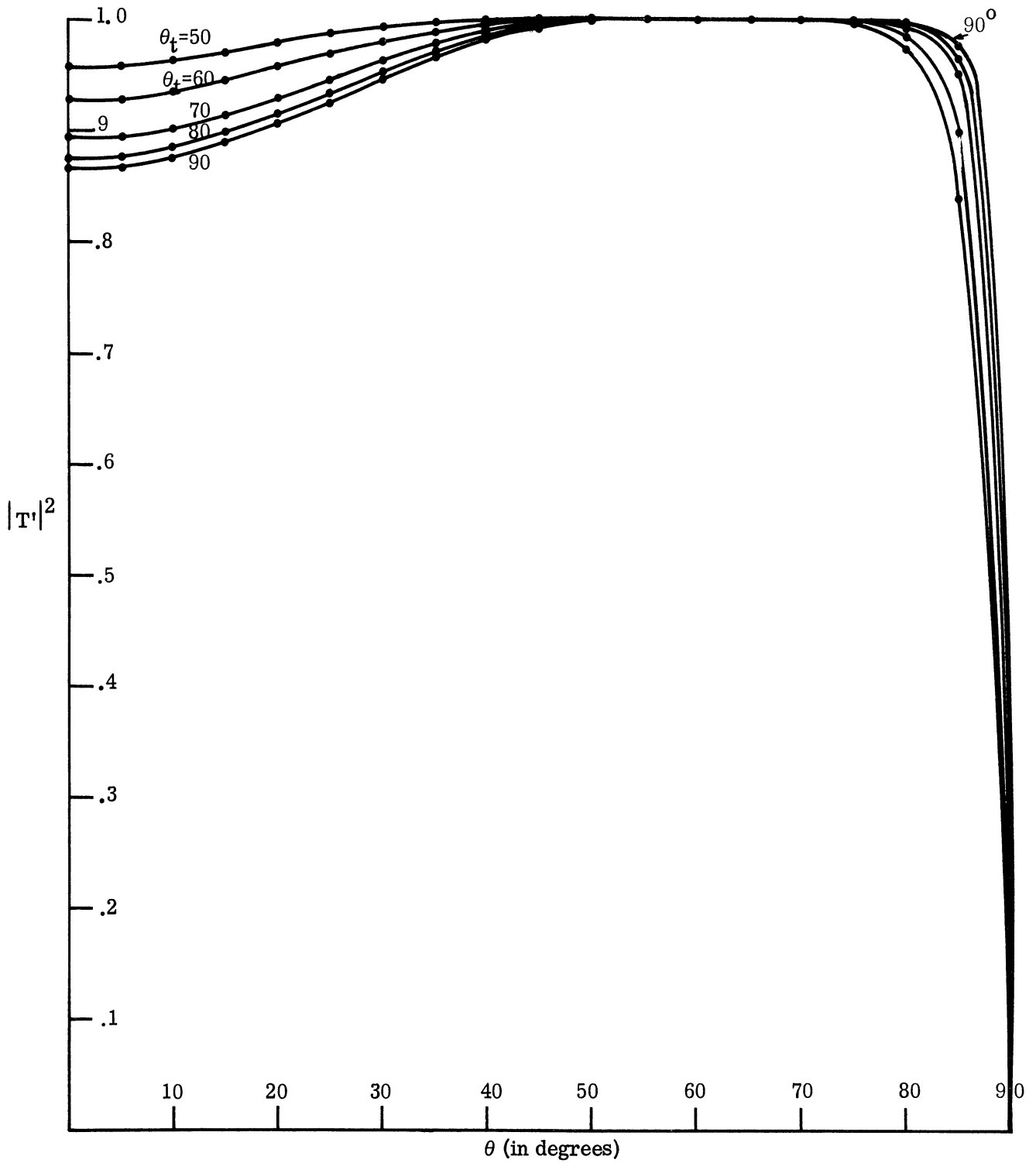


FIG. 3-34: TRANSMISSION COEFFICIENT $|T|^2$ FOR $\epsilon_r = 4$, $\epsilon_{1r} = 6.6$, $\mu_{1r} = .755$, $\alpha' = 90^\circ$ AND VARIOUS VALUES OF θ_t

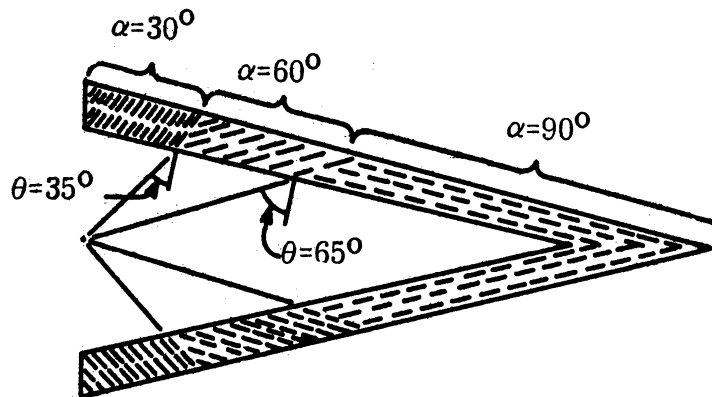


FIG. 3-35: ANISOTROPIC CONICAL RADOME WITH VARIABLE PRINCIPAL AXIS ORIENTATION (α).

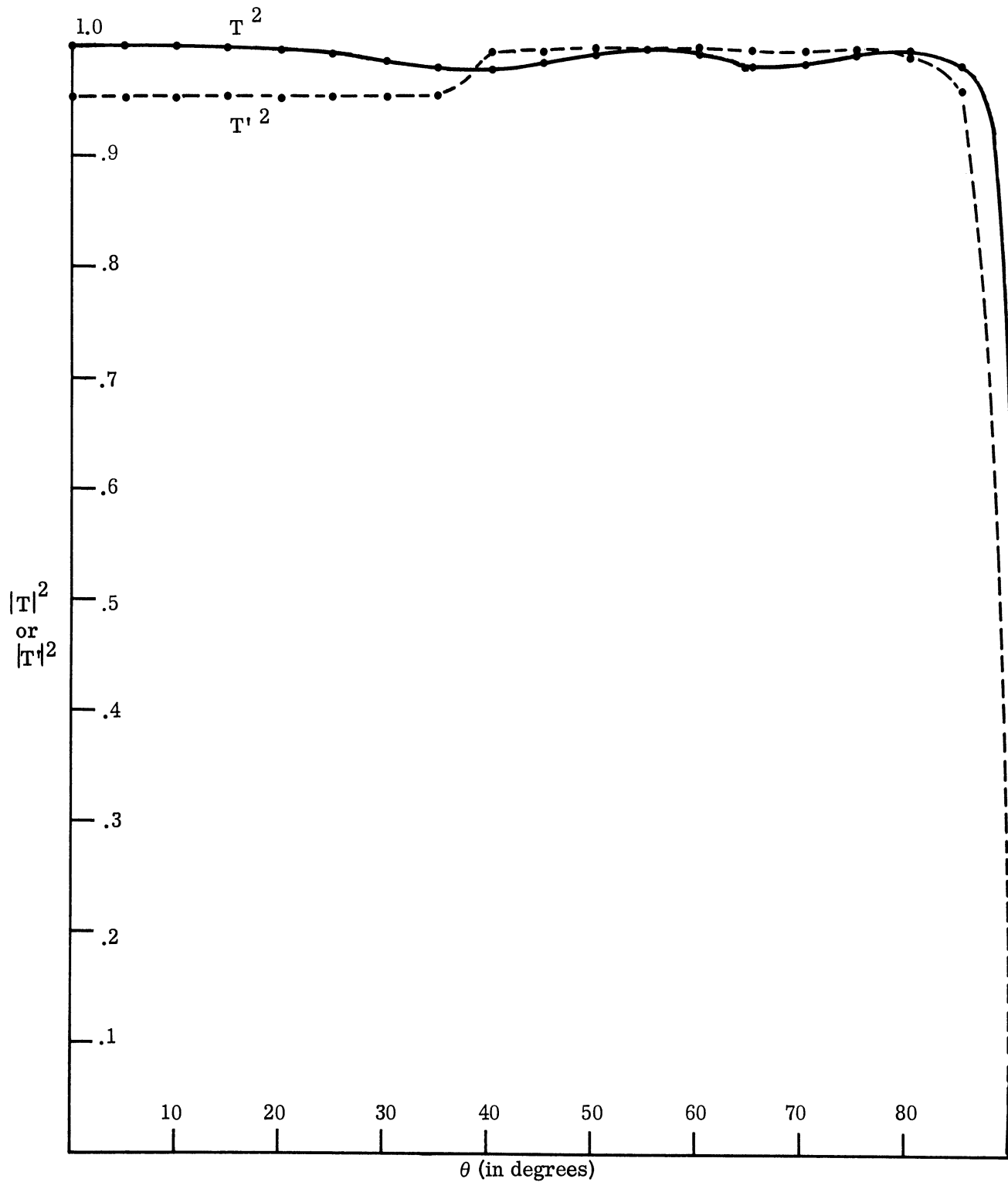


FIG. 3-36: TRANSMISSION COEFFICIENTS $|T|^2$ AND $|T'|^2$ FOR $\epsilon_r=4$, $\epsilon_{1r}=6.6$, $\mu_{1r}=.755$ AND $\theta_t=80^\circ$ WITH α DEPENDENT ON θ .

IV

CONCLUSIONS AND RECOMMENDATIONS

Theoretical study on the transmission of a plane wave through an anisotropic panel indicates that the transmission efficiency depends on the orientation of the principal axis, and better transmission efficiency is obtained, especially for high incident angles, when the principal axis is perpendicular to the plane of the panel. For this orientation it is noted that the physical thickness of the equivalent half wave panel is smallest which may be an advantage where the weight is a major factor in a radome design. It was also noted that the transmission efficiency is degraded at normal incidence, when the principal axis is oriented perpendicular to the plane of the panel. By proper orientation of the principal axis, which depends on the angle of incidence, it is shown that transmission efficiencies greater than 95 per cent could be obtained for both polarizations.

It is recommended that the future work on anisotropic panels include experimental verification of the theoretical predictions. A suggested approach for the experimental work would be to employ some low density foam as the base material. Metallic discs of appropriate diameter would be placed on the surface of the material and sandwiched together to form an anisotropic panel. Two or more configurations may be considered, for example, one in which metallic discs could be oriented with the plane of the discs parallel to the interface and for a second case, the discs would be inclined at the other required angles.

REFERENCE

Tai, C-T, et al, (1965), "Radant Analysis Studies - Interim Report No. 1", The University of Michigan, Radiation Laboratory Technical Report No. 07300-1-T. AD 471813 UNCLASSIFIED

Other Reports Written by The Radiation Laboratory Associated with this Contract

Tai, C-T and E S. Andrade (1965), "Radant Analysis Studies - Interim Report No. 2," The University of Michigan Radiation Laboratory Report 7300-2-T, AD 476 698 UNCLASSIFIED

Tai, C-T (1966), "Radant Analysis Studies - Interim Report No. 3," The University of Michigan Radiation Laboratory Report 7300-3-T, AD 488066 UNCLASSIFIED

Tai, C-T (1966), "Radant Analysis Studies - Interim Report No. 4," The University of Michigan Radiation Laboratory Report 7300-4-T, AD 801269 UNCLASSIFIED

Tai, C-T, E. S Andrade and M. A Plonus (1966), "Radant Analysis Studies" AFAL-TR-66-186, The University of Michigan Radiation Laboratory. Report No. 7300-1-F, AD 486 763 UNCLASSIFIED

Tai, C-T and R M Kalafus (1967), "Radant Analysis Studies", AFAL TR 67-62, The University of Michigan Radiation Laboratory Report 7300-2-F, AD 815541 UNCLASSIFIED

DISTRIBUTION LIST

Destination	Number of Copies
Georgia Institute of Technology Engineering Experiment Station Attn: N. E. Poulos Atlanta, Georgia 30313	1
ITT Research Institute Attn: S. L. Blum, Assistant Director Metals and Ceramics Research 10 West 35th Street Chicago, Illinois 60616	1
Illinois Institute of Technology Antenna Department 1412 Bativa, Box 205 Geneva, Illinois 60134	1
Johns Hopkins University Attn: L. B. Weckesser 8621 Georgia Avenue Silver Spring, Maryland 20910	1
Massachusetts Institute of Technology Lincoln Laboratories Attn: Document Room P. O. Box 73 Lexington, Massachusetts 02173	1
Ohio State University Research Foundation Antenna Laboratory Attn: Dr. C. Levitt 1314 Kinnear Road Columbus, Ohio 43212	1
Aeronca Manufacturing Corporation Attn: Byron Reynolds Middletown, Ohio 45042	1

Destination	Number of Copies
Autonetics Division of North American Aviation Inc Attn: Technical Library Dept 502-41-664, Bldg 202 3370 Miraloma Avenue Anaheim, California 92680	1
Bell Aerospace Corporation Attn: Technical Library (Antenna Section) Buffalo New York 14205	1
Boeing Company Aerospace Division Attn: Robert Sutton M/F Antenna and Radome Unit P. O. Box 3707 Seattle, Washington 98124	1
Boeing Airplane Company Airplane Division Attn: C. D. Lunden P. O. Box 707 Renton, Washington 98055	1
Brunswick Corporation Attn: James Carter 325 Brunswick Lane Marion, Virginia 24354	1
Douglas Aircraft Corporation Antenna Department Attn: G. J. Cassell 3855 Lakewood Blvd Long Beach, California 90801	1
Douglas Aircraft Company, Inc Attn: Technical Library (Antenna Section) 3000 Ocean Park Blvd Santa Monica, California 90405	1

Destination	Number of Copies
Electronic Space Structures Corporation Attn: Joe Vitale Old Powder Mill Road West Concord, Massachusetts 01781	1
Emerson and Cuming Attn: E. J. Luoma 869 Washington Street Canton, Massachusetts 02021	1
General Dynamics Attn: Robert Hallse P. O. Box 1011 Pomona, California 91766	1
General Dynamics/Convair Attn: Gus Tricolos 3302 Pacific Coast Highway P. O. Box 1128 San Diego, California 92112	1
General Dynamics /Fort Worth Attn: J. E. Burroughs Grants Lane, P. O. Box 748 Fort Worth, Texas 76101	1
General Electric Company General Engineering Laboratory Attn: Thomas Jordan 1 River Road Schnectady, New York 12305	1
Grumman Aircraft Engineering Corporation Attn: Technical Library, M/F Avionics Bethpage, New York 11714	1
Hughes Aircraft Corporation Attn: Robert Jones Centinela and Teale Streets Culver City, California 90232	1

Destination	Number of Copies
The Martin Company Attn: Technical Library (M/F Microwave Laboratory) Box 5837 Orlando, Florida 32805	1
The Martin Company Attn: Technical Library (Antenna Section) Baltimore, Maryland 21203	1
McDonnell Aircraft Corporation Attn: Technical Library (Antenna Section) Municipal Airport Box 516 St. Louis 66, Missouri 63166	1
Mitre Corporation Attn: Technical Library (M/F Electronic Warfare) Middlesex Turnpike P. O. Box 208 Bedford, Massachusetts 01730	1
Motorola Inc Attn: Antenna Group/Dr. Tice 8201 E McDowell Road Phoenix, Arizona 85008	1
Narmco Industries Inc Attn: Roger Long 8125 Aero Drive San Diego 11, California 92123	1
Raytheon Company Missile Systems Division Radome Section Attn: Robert O. Howe Bedford, Massachusetts 01730	1

Destination	Number of Copies
Technical Research Group Attn: Librarian Antenna Section 130 Constitution Drive Menlo Park, California	1
Director AUL (31-AVE-51-30) Maxwell AFB Alabama 36112	1
DDC Cameron Station Alexandria, Virginia 22314	20 + card
AFAL (AVWE-3) Wright-Patterson AFB Ohio 45433	75
SEG (SEACA/Mr. George F. Duree) Wright-Patterson AFB Ohio 45433	1
AFAL (AVNT) Wright-Patterson AFB Ohio 45433	1
AFCLR (CRRD) L. G. Hanscom Field Bedford, Massachusetts 01730	1
APGC (PGVEP-3) Eglin AFB Florida 32542	1
AFMTC (Technical Library) Patrick AFB Florida 32925	1
AFMDC (Technical Library) Holloman AFB New Mexico 88330	1
Central Intelligence Agency Code SAN 2430 E St SW Washington DC 20505	1
Director Ballistics Research Laboratory Attn: Ballistics Measurement Laboratory Aberdeen Proving Ground, Maryland 21005	1

Destination	Number of Copies
Commander US Army White Sands Signal Agency Attn: SIGWS-FC-02 White Sands, New Mexico 88002	1
US Naval Ordnance Laboratory Attn: Paul Fisher Attn: Code LX/G. N. Plotkin White Oak Silver Springs, Maryland	1
US Naval Research Laboratory Attn: Dr. A. E. Marston Code 5250 Washington DC 20390	1
National Bureau of Standards Department of Commerce Attn: Dr. A. G. McNish Washington DC	1
Chief, Technical Library Office of Assistant Secretary of Defense (R and D) Room 3E1065 Washington DC 20330	1
Scientific and Technical Information Facility Attn: NASA Representative (SAK/DL) P. O. Box 5700 College Park, Maryland 20740	1
Chief, Bureau of Naval Weapons Attn: RRMA-31/Charles Bersch Washington DC 20370	1
AFWL (WLRJ/Mr. W. J. Moulds) Kirtland AFB New Mexico 87117	1
Commander AF Office of Scientific Research Attn: SREC Washington DC	1

8664-1-F

Destination	Number of Copies
NADC Attn: George Tatnell Johnsville, Pennsylvania 18974	1
RTD (RTTH) Bolling AFB DC 20332	1
	<hr/> 145

DOCUMENT CONTROL DATA - R & D

(Security classification of title, body of abstract and indexing annotation must be entered when the overall report is classified)

1. ORIGINATING ACTIVITY <i>(Corporate author)</i> The University of Michigan Radiation Laboratory, Dept. of Electrical Engineering, 201 Catherine Street, Ann Arbor, Michigan 48108		2a. REPORT SECURITY CLASSIFICATION UNCLASSIFIED	
		2b. GROUP	
3. REPORT TITLE ADVANCED RADANT STUDIES - II			
4. DESCRIPTIVE NOTES <i>(Type of report and inclusive dates)</i> FINAL REPORT 1 February - 1 November 1967			
5. AUTHOR(S) <i>(First name, middle initial, last name)</i> Boppana, L. J. Rao			
6. REPORT DATE December 1967	7a. TOTAL NO. OF PAGES 58	7b. NO. OF REFS 1	
8a. CONTRACT OR GRANT NO. F 33615-67-C-1444	9a. ORIGINATOR'S REPORT NUMBER(S) 8664-1-F		
b. PROJECT NO. 416102	9b. OTHER REPORT NO(S) <i>(Any other numbers that may be assigned this report)</i>		
c. Task No. 4161	AFAL-TR-67- 309		
10. DISTRIBUTION STATEMENT This document is subject to special export controls and each transmittal to foreign governments or foreign nationals may be made only with prior approval of AFAL (AVWE-3), Wright- Patterson AFB, Ohio 45433			
11. SUPPLEMENTARY NOTES		12. SPONSORING MILITARY ACTIVITY Air Force Avionics Laboratory Research and Technology Division, AFSC Wright-Patterson AFB, Ohio 45433	

13. ABSTRACT

The transmission characteristics of an anisotropic panel formed by conducting discs are investigated theoretically for different orientation of the principal axis of the medium. The results indicate that the best transmission efficiency is obtained for high incident angles when the principal axis is oriented in such a way that it is perpendicular to the plane of the panel. It is shown that by adjusting the orientation of the principal axis according to the incident angle, better and more uniform transmission could be obtained through radomes of conical structure.

14.	KEY WORDS	LINK A		LINK B		LINK C	
		ROLE	WT	ROLE	WT	ROLE	WT
	<p>RADOME ANISOTROPIC PANEL ARTIFICIAL DIELECTRIC TRANSMISSION EFFICIENCY</p>						

UNIVERSITY OF MICHIGAN



3 9015 03525 0623